

Contents lists available at ScienceDirect

Petroleum Science

journal homepage: www.keaipublishing.com/en/journals/petroleum-science



Original Paper

Characterization and optimization of oil—gas interfacial tension during CO_2/N_2 injection in heavy oil reservoirs: Experimental study and regression model



Chao Zhang ^{a, b, *}, Chao Yu ^{a, b}, Zi-Han Gu ^{a, b}, Kun Liu ^c, Ping-Keng Wu ^d, Zhao-Min Li ^{a, b, e}

- ^a Key Laboratory of Unconventional Oil & Gas Development (China University of Petroleum (East China)), Ministry of Education, Qingdao, 266580, Shandong, PR China
- ^b School of Petroleum Engineering, China University of Petroleum (East China), Qingdao, 266580, Shandong, PR China
- ^c China National Logging Corporation, Southwest Branch, Chongging, 400021, PR China
- d Department of Chemical Engineering, Illinois Institute of Technology, Chicago, IL, 60616, United States
- ^e Bingtuan Energy Development Institute, Shihezi University, Shihezi, 832000, Xinjiang, PR China

ARTICLE INFO

Article history: Received 23 October 2024 Received in revised form 21 March 2025 Accepted 24 March 2025 Available online 25 March 2025

Edited by Yan-Hua Sun

Keywords: CO₂/N₂ Interfacial tension Correlation IFT cloud map Multiparameter

ABSTRACT

CO₂/N₂ injection in heavy oil reservoirs has been demonstrated to enhance oil recovery (EOR) and facilitate CO₂ capture, utilization, and storage (CCUS). Interfacial tension (IFT) is a crucial parameter for characterizing oil recovery, but it can be influenced by real-time changes in reservoir pressure and temperature during gas injection. The impact of the CO₂/N₂ ratio on the oil-gas IFT under varying temperature and pressure conditions remains unclear. Therefore, a systematic study was conducted to investigate the effects of multiple parameters on the oil-gas IFT during development processes, and a three-dimensional (3D) database and a regression model of IFT were established using experimental data. The results show that IFT is strongly correlated with density difference, moderately correlated with pressure and CO2 proportion, weakly correlated with saturates content and resin content, and nonlinearly correlated with temperature, aromatics content, and asphaltene content, respectively. Moreover, it has been observed that an increase in pressure or CO2 proportion can lead to a reduction in IFT. However, the impact of temperature changes on IFT varies across different pressure ranges. We introduce a new parameter, the equivalent interfacial tension pressure during temperature changes (EITP), to characterize this effect and discuss the reasons for the emergence of EITP, providing new insight into optimizing the CO₂/N₂ injection ratio in the reservoir. This study aims to reveal the advantages of oil—gas interface characteristics under the influence of multiple parameters in promoting low-carbon and efficient development of heavy oil reservoirs, and to explore the significance of CO₂/N₂ for enhancing heavy oil recovery.

© 2025 The Authors. Publishing services by Elsevier B.V. on behalf of KeAi Communications Co. Ltd. This is an open access article under the CC BY-NC-ND license (http://creativecommons.org/licenses/by-nc-nd/4.0/).

1. Introduction

Global energy consumption has long been a key focus of the international community. The demand for fossil fuels continues to rise with the growth of the global economy and population, and the development of unconventional oil and gas has become a current research hotspot (Johnsson et al., 2019; Liu et al., 2024). According to the latest data from the International Energy Agency (IEA) in

estimated global crude oil resources currently range from 9 to 11 trillion barrels, with over two-thirds classified as heavy oil. Heavy oil is mainly found in Venezuela, Canada, the United States, China, and is widely used in transportation, the chemical industry, and construction materials. Efficient development of heavy oil will be crucial in meeting the increasing energy demand in the coming years. Special techniques are necessary for heavy oil development. Presently, the most effective production methods include steam flooding (SF), cyclic steam stimulation (CSS), steam-assisted gravity

drainage (SAGD), and fire flooding (FF) (Dong et al., 2019;

2024, fossil energy, which predominantly comprises oil and gas, will account for up to 80% of global resource consumption. The

E-mail address: zhangc@upc.edu.cn (C. Zhang).

^{*} Corresponding author.

Mokheimer et al., 2018; Zhang et al., 2024c). These methods involve injecting high-temperature media or initiating in-situ combustion to reduce crude oil viscosity, improve fluid properties, and enhance oil recovery (EOR). Nonetheless, these efficient recovery methods often require substantial thermal energy input, including heat generation, transfer, and exchange, making thermal recovery operations energy-intensive (Bera and Babadagli, 2015; Hasanvand and Golparvar, 2014; Leung et al., 2014). Moreover, considering the reservoir's effective thickness, considerable depth, and diverse rock and fluid conditions, the heating method may not be suitable for certain heavy oil reservoirs, necessitating the exploration of alternative cold production methods.

In the context of carbon capture, utilization, and storage (CCUS), CO₂-EOR injection is widely used in various reservoirs and is currently one of the most effective production technologies (Alvarado and Manrique, 2010). CO₂ injection not only enhances oil recovery but also facilitates long-term CO2 storage and mitigates greenhouse gas emissions (Zhang et al., 2024b). CO₂ can enter a supercritical state (31 °C, 7.29 MPa) under the original oil reservoir conditions and possesses strong dissolving and extraction capabilities. After multiple contacts with crude oil, CO₂ dissolves into the crude oil, resulting in oil expansion, decreased oil density (ρ) , viscosity (μ) , interfacial tension (σ) , and increasing the number of oil displacement capillaries (Bautista et al., 2014). Hwang and Ortiz (2000) noted that CO₂ exhibits robust extraction capabilities for light components in crude oil, with extraction efficiency increasing with pressure. In conventional light oil reservoirs, the extraction mechanism of CO₂ is the primary influencing factor of EOR. After contact with crude oil, CO2 consistently dissolves and extracts light components into the gas phase. Orr and Taber (1984) conducted research on CO₂-EOR and pointed out that higher pressure enhances the efficiency of CO₂ oil displacement. When the reservoir pressure exceeds the minimum miscible pressure (MMP), miscible flooding can occur, the interfacial tension (IFT) between oil and gas to zero, and recovery can reach up to 90% with a 1.2 pore volume (PV) injection. Chen et al. (2022) conducted CO₂ core displacement experiments and found that the seepage capacity of reservoir fluids can be enhanced significantly by strong and sufficient interactions of CO₂ and oil. The mass transfer effect between CO₂ and crude oil can be improved by taking appropriate measures to shut the well, allowing the deadend oil in the pore to be utilized. In heavy oil reservoirs, the dissolution mechanism of CO₂ predominantly influences EOR. Li et al. (2012) analyzed the high-pressure properties of CO2 and heavy oil, noting continuous CO2 dissolution upon contact with crude oil. This process improves the physical properties of heavy oil. During production, dissolved gas molecules in the oil expand and displace crude oil, a process known as CO2 huff and puff (Nguyen et al., 2018). However, due to the limited presence of light components in heavy oil, achieving miscible production through CO₂ injection is challenging. Furthermore, the light and medium components in heavy oil decrease upon multiple contacts, deteriorating the physical properties of the remaining oil and posing challenges for CO₂ injection development in later stages (Abedini and Torabi, 2014; Liu and Rui, 2022).

Flue gas primarily consists of CO_2 and N_2 . Utilizing flue gas flooding technology in heavy oil reservoirs can enhance the economic benefits of the oil field at a reduced cost (He et al., 2022). Li et al. (2018) investigated the effects of CO_2/N_2 injection on the physical properties of crude oil in the reservoir. CO_2 exhibits superior dissolving and extraction capabilities compared to N_2 , whereas N_2 can elevate formation pressure and maintain oil production rates. Additionally, the inclusion of N_2 can reduce the extraction capacity of CO_2 . While enhancing solubility, it can also

prevent the loss of light and medium components in crude oil. This helps to avoid the problem of production decline caused by the precipitation of heavy components (Alvarado and Manrique, 2010; Bender and Akin, 2017; Liu and Rui, 2022). Zhang et al. (2024b) has studied the impact of N₂ as an impurity gas on CO₂ storage performance, elucidating the safety and sustainability of CO₂ storage from the perspective of gas—liquid—solid interactions. Adding nitrogen to CO₂ creates additional dissolution pits on the calcite surface, facilitating greater CO₂ storage column heights. Studying the impact mechanism of different parameters on the oil-gas interface will not only help enhance oil recovery, decrease production costs, but also reduce greenhouse gas emissions and promote the sustainable development of the oil industry (Ma et al., 2023). Researchers are increasingly focusing on the measurement and control of oil-gas IFT to better understand its role in reservoir development (Wang et al., 2023; Yang and Gu, 2005; Yang et al., 2015; Zhang et al., 2020). Yang and Gu (2005) analyzed the impact of pressure on CO₂/oil IFT, pointing out that higher pressure enhances the abilities of CO2 diffusion and dissolution, leading to a greater decrease in IFT. The effect of temperature on oil-gas IFT is complex. Zolghadr et al. (2013a) studied the influence of temperatures on oil-gas IFT, noting that the change pattern of IFT with temperature is not uniform. Shang et al. (2017) investigated the IFT of CO₂/N₂ (3:1) mixed gas with paraffin and found that adding N2 increases the IFT. The higher the N2 content in the gas, the weaker the oil-gas interface effect (Gajbhiye, 2020).

Up to now, research has mainly focused on the impact of individual parameters on IFT, with limited investigations examining the combined effects of multiple parameters on oil-gas IFT. Moreover, IFT models that simultaneously consider crude oil characteristics, temperature, pressure, and CO₂/N₂ ratio are not widely used. The conventional IFT model for gas-alkane systems are primarily derived from gradient theory (GT), linear gradient theory (LGT), and density gradient theory (DGT), which focus on binary components of pure fluids (Enders and Quitzsch, 1998; Zuo and Stenby, 1996, 1997). Due to the complexity of crude oil, it is very challenging to establish an IFT model that considers not only the interaction between crude oil components, but also gas dissolution, mass diffusion, and extraction effects in crude oil. Big data fitting is a method that involves training and testing on known experimental data to construct prediction models that can describe patterns within the data. It aims to predict unknown data by aligning the test data as closely as possible with the actual data (Shorten and Khoshgoftaar, 2019). Recently, some researchers have used big data regression to establish correlating models for gas-liquid properties, such as solubility, viscosity, and IFT (Behvandi and Mirzaie, 2022; Lv et al., 2023; Mutailipu et al., 2024; Zheng et al., 2023). These models are highly accurate and reliable. Compared to theoretical models, the big data learning approach utilizes data trends to identify the optimal fitting formula, minimizing fitting errors to the greatest extent. In this study, experiments on oil-gas IFT under different temperatures, pressures, and CO₂ ratios were conducted, and an IFT regression model considering multiple parameters was established. Additionally, a threedimensional database of IFT, based on experimental data, was constructed to generate two-dimensional cloud maps of IFT under constant temperature, pressure, and CO₂ proportion. The mechanism of the combined effects of multiple parameters on IFT was analyzed. Finally, a new approach for optimizing CO₂/N₂ injection ratios in various reservoirs was developed based on the distribution pattern of IFT in the three-dimensional database, and the findings provide significant theoretical guidance implications for gas injection EOR.

2. Experimental

2.1. Experimental sample

Crude oil was collected from the Shengli Oilfield in China, and experimental CO_2 and N_2 with purity greater than 99.99%, were provided by Qingdao Kerun East New Energy Co., LTD. The carbon number distribution of the oil, determined via gas chromatography, is shown in Fig. S1(a). Viscosity measurements were taken with an Anton Paar MCR 301 Rheometer over a temperature range of 19.8–150 °C, as shown in Fig. S1(b). The saturates, aromatics, resin, and asphaltene (SARA) content was measured according to the NB/SH/T 0509 petroleum four-component analysis standard, as shown in Fig. S1(c). The density of dead oil at a temperature range of 60–140 °C was measured using an Anton Paar DMA Densitometer, as demonstrated in Fig. S1(d). For specific details, please refer to the Supporting Information.

2.2. Experimental principles and methods

The pendant drop method uses image contour fitting and the Young—Laplace equation to calculate the IFT of a liquid droplet (Andreas et al., 1938), as shown in Eq. (1).

$$\frac{\mathrm{d}(x\sin\theta)}{x\mathrm{d}x} = \frac{2}{r} - \frac{\Delta\rho gz}{\gamma} \tag{1}$$

where x and z are parameters describing the droplet morphology, representing the equivalent dimensions of the droplet in the horizontal and normal directions, respectively; θ represents the running angle of the droplet profile; r is the curvature radius of the droplet; $\Delta \rho$ denotes the density difference between oil and gas; g represents the gravitational acceleration.

The IFT measurements were influenced by the droplet morphology, the running angle between the droplet and needle, and the density difference between the gas and liquid phases. It was crucial to position the camera horizontally and input the correct densities for the saturated crude oil and gas phase. When unsaturated crude oil enters the gas phase, the oil-gas interface undergoes bidirectional mass transfer, dissolution, and extraction of CO₂. The dissolution process increases the liquid phase volume and decreases oil density, while the extraction process transfers light components from the oil phase to the gas phase, enriching the gas phase and increasing its density. Since heavy oil contains negligible light components and the increase in gas phase density is minimal, the oil phase density is a key factor affecting IFT. The PVT method was used to determine the crude oil density. Fig. 1(a) shows the ultra-high pressure fully visible PVT test system (Sanchez Technology, France), which includes a 250-mL high-temperature high-pressure cell, a stirring system, a heating system, a pressurization system, a volume display system, a visual window, and a data acquisition system. After evacuating the cell, a specific mass of crude oil was introduced, followed by the injection of various gases. The fluid in the cell chamber was stirred and rotated, and the oil volume was recorded once equilibrium was reached, as shown in Fig. 1(b). The oil density under different temperature and pressure conditions was calculated using the mass-volume relationship, while the gas phase density was determined using the state equation developed by Span and Wagner specifically for characterizing CO₂ (Span and Wagner, 1996). The gas phase density in mixtures was obtained by combining pure fluids with different molar ratios using a weighted approach. Finally, the density difference between saturated crude oil and gas under varying temperature and pressure conditions was calculated, as shown in Table S1 of the Supporting Information.

The Tracker-H interfacial tensiometer (TECLIS, France) was used to measure IFT between the liquid and gas (Fig. 1(c)). This tensiometer consists of a 750-mL high-temperature high-pressure chamber, an 800-µL injection syringe (1.8 mm needle diameter), a heating control system, temperature probes, a pressure data acquisition system, a high-definition camera, an image capture and processing system, and a data analysis system. The instrument measures relevant parameters using the pendant drop method and the axisymmetric drop shape analysis (ADSA) technique (Zhang et al., 2016). Stable interfaces generally allow for accurate IFT measurement using image recognition technology. However, measurements based on a single image lacked precision due to complex interactions in high-pressure oil-gas interfaces, such as dissolution (Zhang et al., 2023), mass diffusion (Rezk and Foroozesh, 2018), and extraction (Wang et al., 2010), which caused droplet motion within the gas phase. To address this, the dynamic IFT method was employed to measure the equilibrium IFT of oil and gas (Yang and Gu, 2005). Fig. 1(d) illustrates that dynamic IFT data fluctuated over time, with larger variations observed in the initial stage compared to the equilibrium stage, suggesting that averaging over the entire stage could introduce errors. Although oil droplets exhibit dynamic behavior during the IFT measurement, they eventually reach equilibrium after repeated contact with the gas, resulting in a stable equilibrium IFT value. While steady-state oil density can influence the dynamic transition of oil from an unsaturated to a saturated state, it has little effect on the IFT value once equilibrium is reached. To ensure accuracy, nonlinear fitting was performed on the equilibrium stage data from dynamic IFT measurements, and the exact IFT values under various temperature, pressure, and CO₂ molar ratio conditions were determined.

3. IFT model

3.1. Experimental data preprocessing

Fig. 2(a)–(e) shows the IFT curves of oil and gas under different temperatures, pressures, and gas compositions, based on a total of 175 experimental data points. The curves reveal the influence of a single variable on IFT, but the evolution of IFT under the combined effect of the three parameters is difficult to clarify. Thus, a threedimensional (3D) data model was established using the existing IFT data. Initially, 175 experimental scatter points were interpolated using the MATLAB 3D scatter interpolation function to build the 3D model (Amidror, 2002). Numerous reports suggest that the IFT curve of light oil follows a linear pattern (Wang et al., 2023), whereas crude oil exhibits nonlinear patterns in the IFT between oil and gas under high pressure (Kong et al., 2021; Yang et al., 2015; Zhang et al., 2020). Therefore, natural interpolation was used in the data processing to better capture the changes in the oil and gas IFT, resulting in smoother results compared to linear interpolation. The interpolation results, as depicted in Fig. 2(f), expanded the data points from 175 to 4640. This 3D data model visually displays the distribution pattern of low IFT. The low IFT region in the 3D data model corresponds to the smallest area, indicating that its formation is increasingly dependence on low temperature, high pressure, and high CO₂ proportion. The color gradient variation indicates that pressure has the most significant influence on the low IFT region, followed by gas composition, with temperature being the least influential factor. Pressure and gas composition are crucial for the formation of the low IFT region, which cannot form under low pressure and low CO₂ composition. Temperature does not play a decisive role in the formation of the low IFT region, although it becomes difficult to form this low IFT region at excessively high temperatures.

Fig. 3(a) shows IFT isosurfaces under different conditions, where the largest area corresponds to an equivalent IFT of 22 mN/m in the

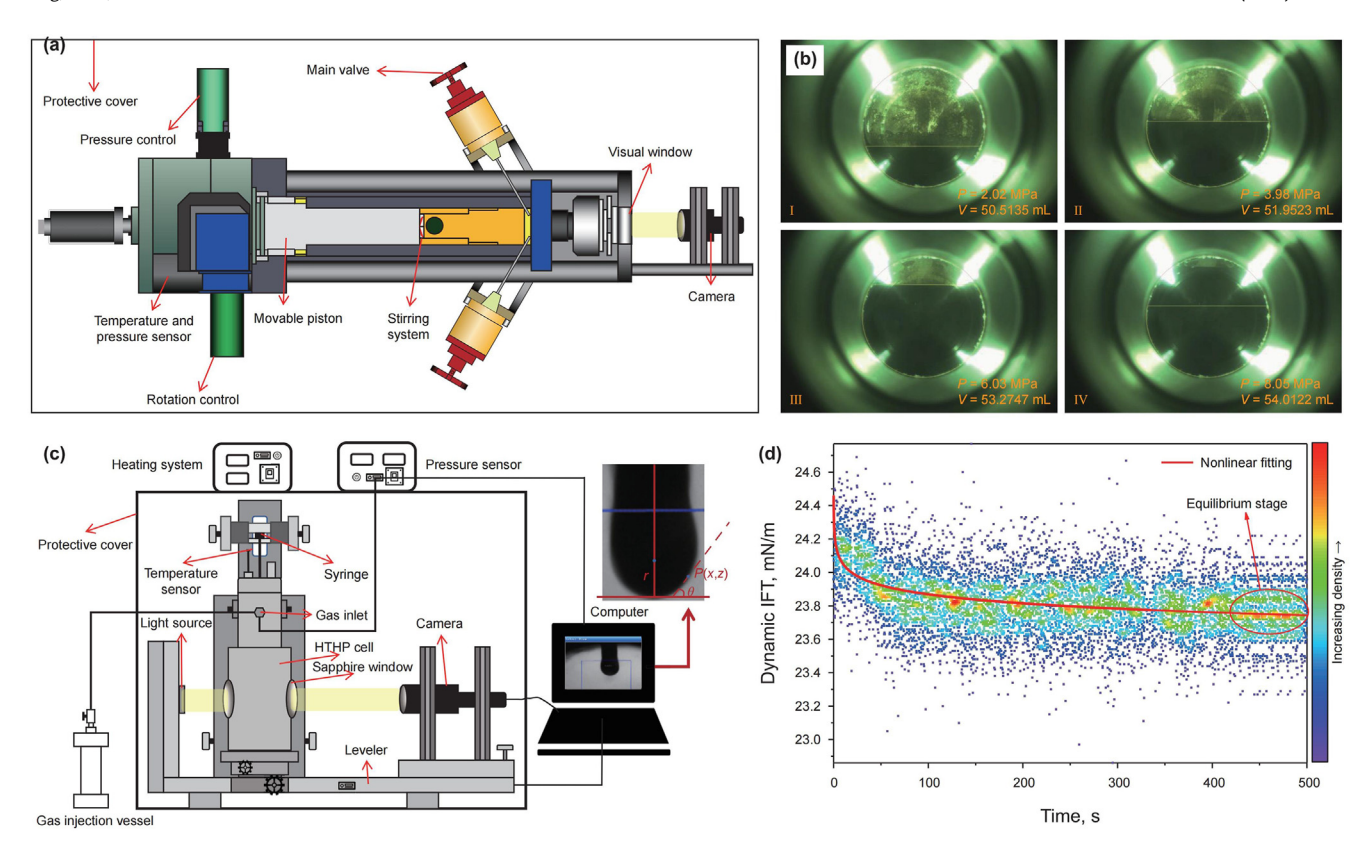


Fig. 1. Oil density and dynamic IFT experiment. (a) Ultra-high pressure fully visible PVT test system; (b) the saturated oil volume under different pressures (CO₂/N₂ molar ratio 1:1, 100 °C); (c) interfacial tension analyzer; (d) dynamic oil—gas IFT (CO₂, 60 °C, 2 MPa).

data model. On this value, multiple methods were available to form this region, with no excessive reliance on any specific parameter. However, as IFT increases or decreases, the conditions for forming For specific details, please refer to the Supporting Information. A multiparameter IFT model is developed using machine learning, as shown in Eq. (2), with the solution given in Eq. (3):

$$\begin{pmatrix} T_{11} & P_{12} & R_{13} & \rho_{14} & Sat_{15} & Aro_{16} & Res_{17} & Asp_{18} \\ \vdots & \vdots & \vdots & \vdots & \vdots & \vdots & \vdots \\ T_{n1} & P_{n2} & R_{n3} & \rho_{n4} & Sat_{n5} & Aro_{n6} & Res_{n7} & Asp_{n8} \end{pmatrix} \times \begin{pmatrix} x_1 \\ \vdots \\ x_8 \end{pmatrix} = \begin{pmatrix} b_1 \\ \vdots \\ b_n \end{pmatrix}$$
 (2)

both low and high IFT regions become more stringent. The areas occupied by both regions decrease, indicating a stronger dependence on specific temperature, pressure, and gas composition. As the low IFT region transitioned to the high IFT region, the equivalent profiles exhibited "folding and bending," which become more pronounced with higher IFT values. This phenomenon indicates that, for a constant parameter, the other two parameters have different degrees of influence on IFT. Therefore, it is necessary to slice the 3D data model and further analyze the impact mechanism of different parameters on IFT using 2D cloud maps, as shown in Fig. 3(b)–(d).

3.2. Model building

This study employs a big data regression method to build an IFT model. The dataset includes 242 data points: 175 from this study and 67 from four types of oil in the literature (Hemmati-Sarapardeh et al., 2013, 2014; Shang et al., 2017; Yang et al., 2015). The samples are randomly divided into training and testing sets in a 6:4 ratio.

where T, P, R, ρ , Sat, Aro, Res, and Asp represent temperature (°C), pressure (MPa), CO_2 proportion (molar fraction), oil—gas density difference (g/cm^3), saturates content (mass fraction), aromatics content (mass fraction), resin content (mass fraction), and asphaltene content (mass fraction), respectively. These are the independent variables of the model, controlled by the coefficient matrix, while the dependent variable is IFT (mN/m), denoted as b. The undetermined coefficient matrix is represented by x.

$$Y = \sum_{i=1}^{n} \beta_i X_i + \varepsilon \tag{3}$$

where n equals 8; the independent variable is denoted as X_i ; the dependent variable Y as IFT; and the unknown coefficients to be determined as β ; ε represents the deviation between the experimental and predicted values.

The equation is solved using Python's linear regression function, based on the least square method. It fits the data by minimizing the

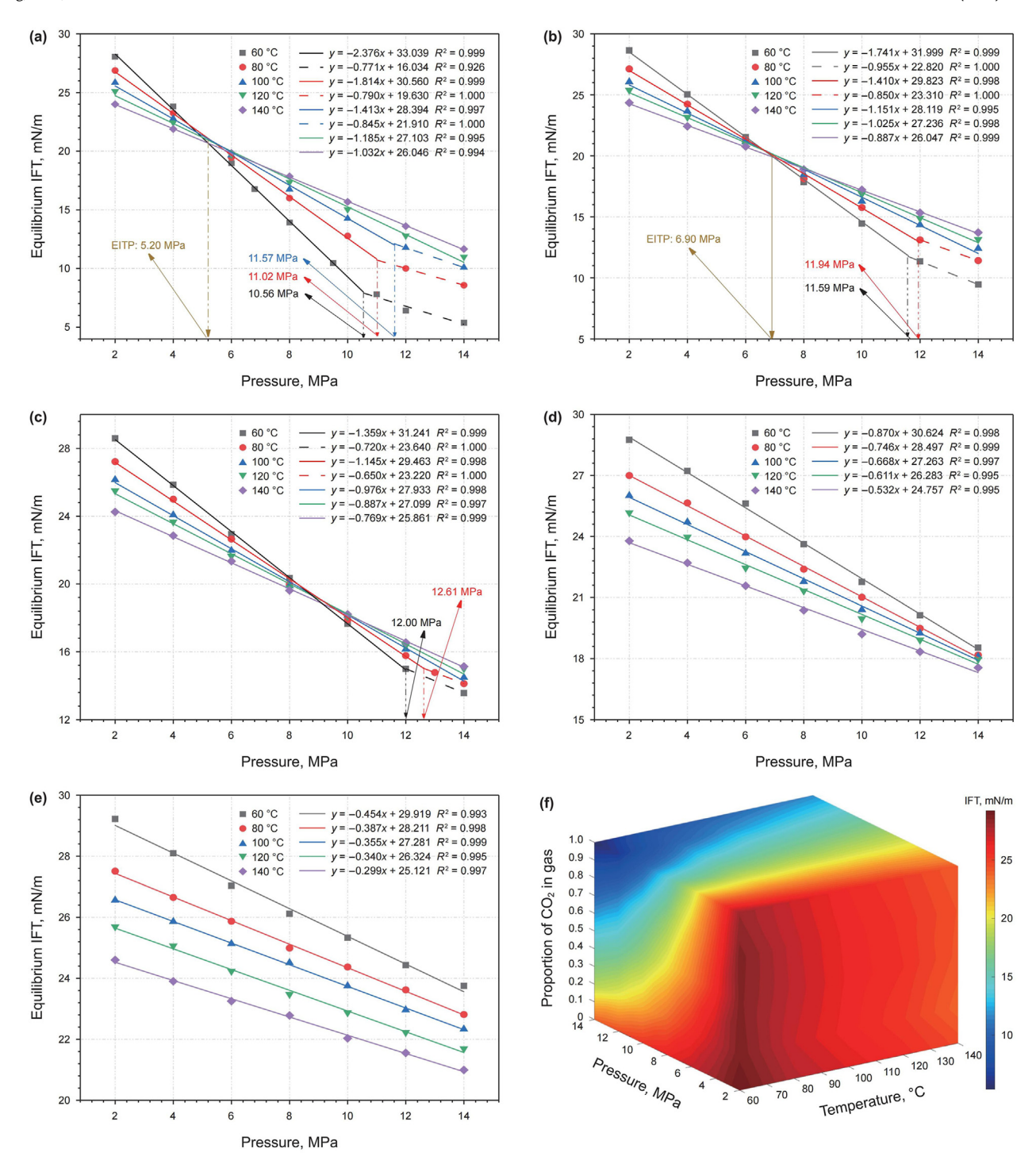


Fig. 2. Equilibrium IFT of oil—gas at different temperatures, pressures, and gas compositions. (a) CO₂; (b) CO₂/N₂ (3:1); (c) CO₂/N₂ (1:1); (d) CO₂/N₂ (1:4); (e) N₂; (f) IFT 3D model.

sum of squared residuals between observed values and the predicted values made by the regression model. The optimal coefficients β_1 – β_8 were obtained using the stochastic gradient descent algorithm (Shalev-Shwartz and Zhang, 2013). These coefficients are then used to introduce independent variables into the model for predicting the dependent variable, improving the accurate of the IFT model. The first-order regression coefficients are presented in Table 1, with results shown in Fig. 4(a1).

The first-order IFT model had unsatisfactory accuracy, with a coefficient of determination (R^2) of 0.885. In the linear regression, the values of β_5 – β_8 were much larger than β_1 – β_4 , indicating that

the intrinsic characteristics (SARA) of crude oil have a greater impact on IFT, while external characteristics (T, P, R, ρ) contribute less. The first-order model may not adequately capture the influence of external conditions on IFT. To improve accuracy, data expansion is necessary to increase the contribution of external characteristics. This involves upgrading the regression from first-order to higher-order, expanding parameters with high influence but low contribution to better elucidate the relationship between these parameters and IFT, improving fitting accuracy and reducing the risk of overfitting (Bansal et al., 2022; Garcea et al., 2023). By self-multiplying and cross-multiplying T, P, R, and ρ , the 8

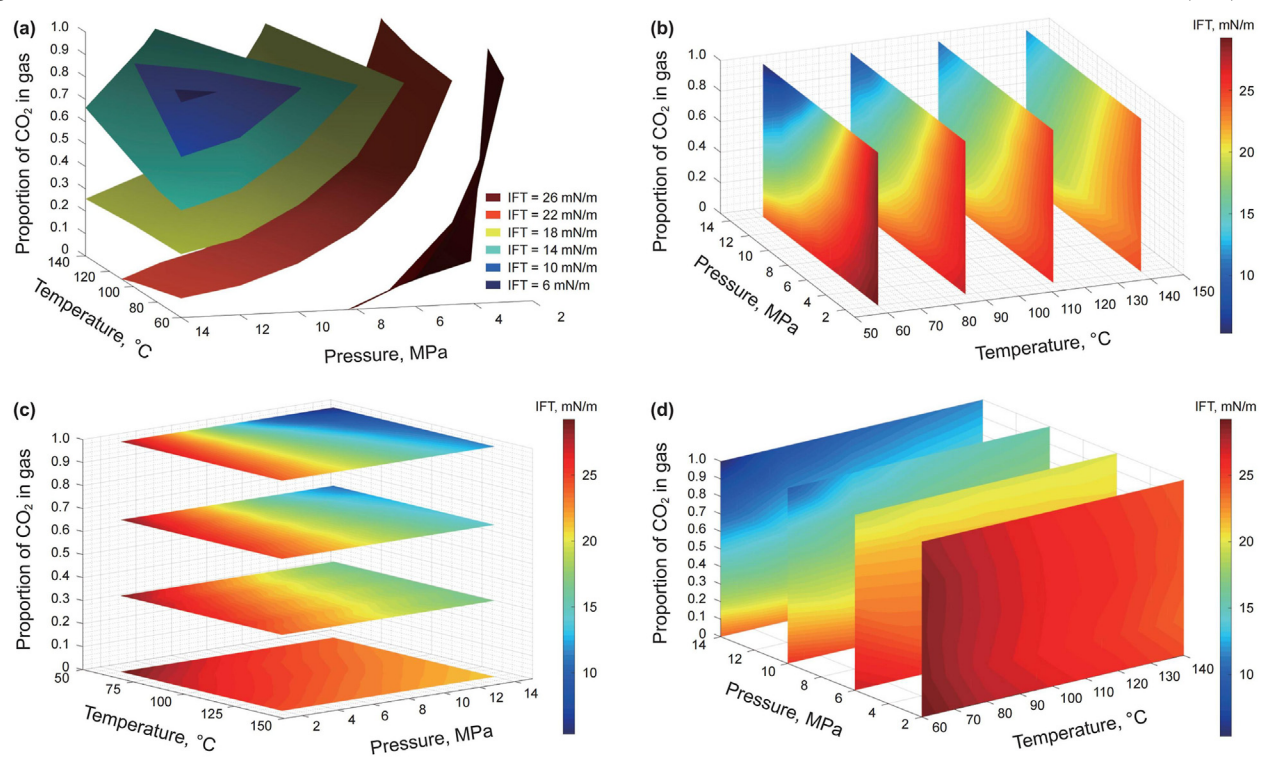


Fig. 3. IFT profiles under different conditions. (a) Different IFT isosurfaces using three-dimensional interpolation; (b) temperature variation (60, 86.6, 113.3, and 140 °C); (c) gas composition variation; (d) pressure variation (2, 6, 10, and 14 MPa).

coefficient columns are expanded to 18, as shown in Eq. (4). The solution is expressed in Eq. (5).

where n equals 8; m equals 4.

As shown in Fig. 4(a2) and Table 2, performing a second-order expansion on temperature, pressure, gas composition, and density difference data, significantly improved the coefficient matrix.

$$Y = \sum_{i=1}^{n} \beta_{i} X_{i} + \beta_{n+1} TP + \beta_{n+2} TR + \beta_{n+3} T\rho + \beta_{n+4} PR + \beta_{n+5} P\rho$$

$$+ \beta_{n+6} R\rho + \sum_{i=1}^{m} b_{n+i+6} X_{i}^{2} + e$$
(5)

The R^2 value of the test set increased from 0.885 to 0.980. As prediction accuracy improved, the number of coefficients increased from 8 to 18, making the model more complex and necessitating more parameters to explain data changes and accommodate a broader range of data features. Specifically, after data expansion, the coefficients for T, P, and R increased, while those for SARA decreased. The contribution of density difference shifted from ρ to ρ^2 , and its coefficients also decreased. This suggests that data

Statistics of first-order IFT model coefficients.

β_1	eta_2	β_3	eta_4	ε	Training R ²	Testing R ²
-0.007398800	0.0124184468	-1.91495184	57.0181457	-175.7307630	0.95711	0.88455
β_5	eta_6	β_7	β_8			
155.848965	126.319405	163.818774	182.063177			

expansion balanced the dataset by generating more samples for underrepresented classes, thereby enhancing the ability of model to learn from all classes. A comparison of regression coefficients revealed that the influence of physical quantities on IFT is not entirely linear. The effects on IFT can be categorized as linear $(\beta_1-\beta_8)$, synergistic $(\beta_9-\beta_{14})$, and quadratic $(\beta_{15}-\beta_{18})$. The mass fraction of resin (*Res*) mainly influences the linear effect, while

density difference (ρ^2) dominates the quadratic effect. The product of density difference and CO_2 proportion $(R\rho)$ dominates the synergistic effect by balancing the linear and quadratic effects. To further quantify the correlation between physical quantities and IFT, the Pearson correlation coefficients between various parameters were calculated, as shown in Fig. 4(b), with the calculation principle in Eq. (6).

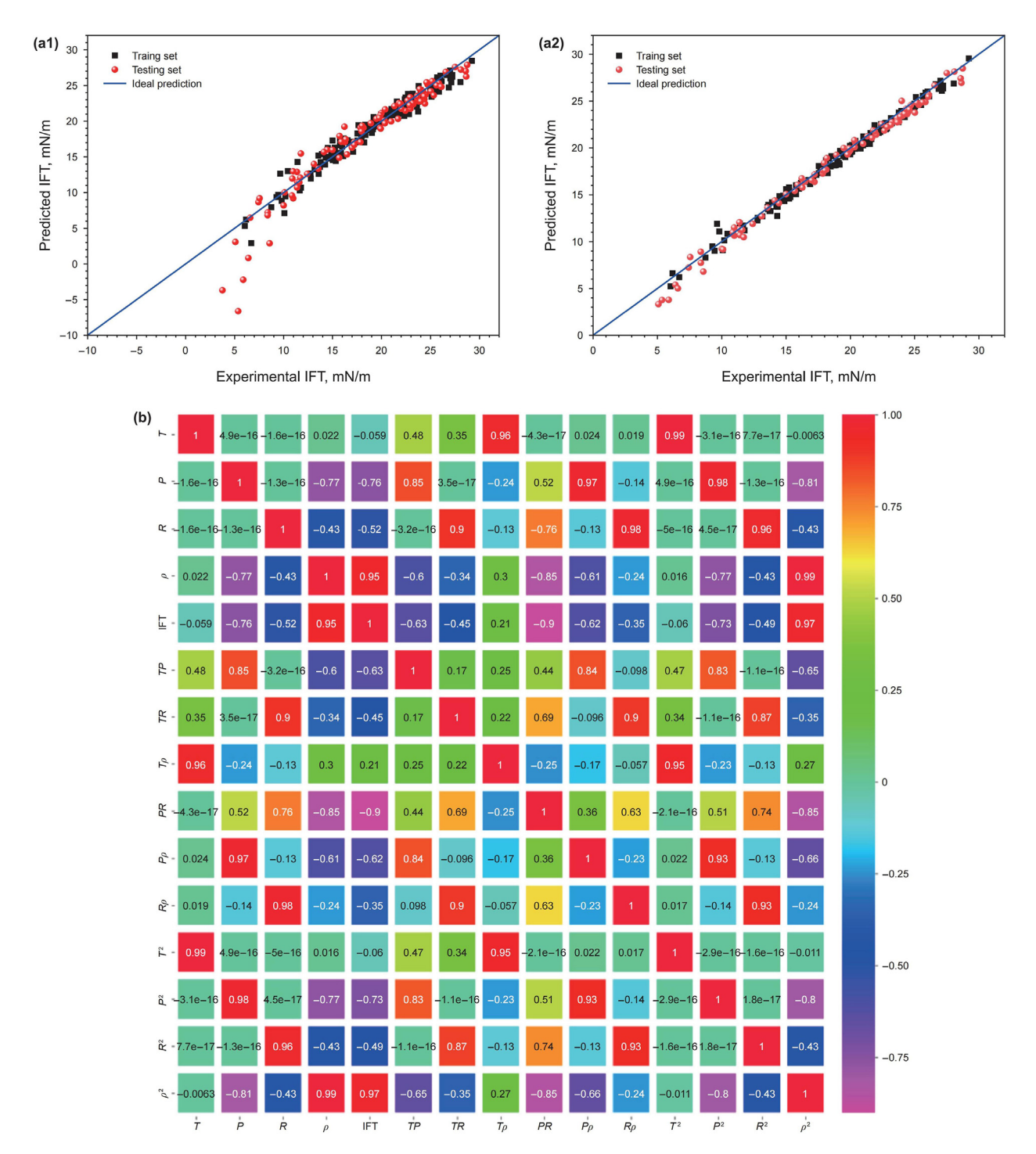


Fig. 4. Accuracy and correlation analysis of IFT model. The testing results and correlation analysis of the first-order model (**a1**) and the second-order model (**a2**). (**b**) shows Pearson correlation coefficients between different regression parameters, with $|r| \le 0.3$ indicating non-linear correlation, $0.3 < |r| \le 0.5$ indicating weak linear correlation, $0.5 < |r| \le 0.8$ indicating moderate linear correlation, and |r| > 0.8 indicating strong linear correlation.

 Table 2

 Statistics of second-order IFT model coefficients.

β_1	eta_2	eta_3	eta_4	eta_5	β_6	β_7
0.183798469	0.945981664	-2.77085425	1.59128521	126.948335	104.200659	143.448027
β_8	β9	β_{10}	β_{11}	β_{12}	β_{13}	β_{14}
141.241071	-0.0007824677	0.035094729	-0.226774409	-0.7013008	-0.959017462	-2.95732818
β_{15}	β_{16}	β_{17}	β_{18}	ε	Training R ²	Testing R ²
-0.000072043	-0.00416875	3.31988317	42.8314785	-132.98880493	0.99033	0.98011

$$r = \frac{\sum_{i=1}^{N} (x_i - \overline{x})(y_i - \overline{y})}{\sqrt{\sum_{i=1}^{N} (x_i - \overline{x})^2 \sum_{i=1}^{N} (y_i - \overline{y})^2}}$$
(6)

where x represents the independent variable and y represents the dependent variable; \overline{x} and \overline{y} are the means of the independent and dependent variables, respectively; x_i and y_i represent the values of the independent and dependent variables for the ith data point.

A significant positive correlation between IFT and density difference is evident, with a Pearson correlation coefficient (PCC) of 0.91. Squaring the density difference maximizes the correlation between IFT and ρ^2 , yielding a PCC of 0.93. At this point, the variation trend of IFT is almost consistent with ρ^2 , indicating a pronounced quadratic correlation between IFT and density difference. However, the correlation between temperature and IFT is minimal, with a PCC of only 0.1, suggesting that temperature affects IFT differently from other variables. Further investigation into the temperature-IFT relationship is warranted. Additionally, IFT exhibits a moderate negative correlation with pressure (PCC of 0.63) and CO₂ proportion (PCC of 0.54). After squaring pressure and CO₂ proportion, the correlation between pressure and IFT decreased, while the correlation between CO₂ proportion and IFT slightly increased. The absolute values of the PCCs were 0.60 and 0.55, respectively, indicating that only part of the IFT curve corresponds to variations in pressure and CO₂ proportion. Notably, both pressure and CO₂ proportion are moderately negatively correlated with IFT, while the product of pressure and CO2 proportion (PR) exhibits a strong negative correlated with IFT (PCC of 0.83). Data expansion generates a new set of highly correlated samples, allowing the model to better explore the functional relationship between independent and dependent variables. The correlation between crude oil composition (SARA) and IFT also varies. The saturated hydrocarbon content is weakly negatively correlated with IFT. CO₂ preferentially extracts compounds with low molecular weights and low degrees of molecular condensation (Ni et al., 2015), meaning that higher saturated component content leads to lower IFT. Resin exhibits the strongest correlation with IFT, demonstrating a weak positive correlation. Resin, as large organic molecules, enhance fluid viscoelasticity, making it harder for CO2 to break their bonds and weakening the interaction between CO₂ and crude oil. The content of aromatics and asphaltene does not correlate linearly with IFT. The aromatics in heavy oil are mainly composed of polycyclic compounds, which easily form hydrogen bonds with other hydrocarbons or adsorb onto macromolecular chains, weakening the extraction effect of CO₂ on aromatics. Experimental data show that Shengli crude oil has high resin content and low asphaltene content. In crude oil, resins tend to form associations with asphaltenes through hydrogen bonding, while smaller aromatics molecular easily penetrate the internal and surface gaps of these resin-asphaltene aggregates, forming more complex structures. This inhibits the dissolution and diffusion of CO₂ in the oil, and results in higher IFT. In

contrast, North American crude oil has high asphaltene content and low resin content. This prevents the formation of such aggregates, leading to a lower IFT during CO₂ injection, accompanied by asphaltene precipitation. Therefore, asphaltene and aromatic contents alone do not determine IFT; the correlation depends on resin content and type.

Comparing the correlation between different parameters and IFT reveals that a higher number of strongly correlated parameters improves prediction accuracy. Medium, weak, and non-linear correlations are also significant. While these parameters may not individually have strong explanatory power, they contribute unique information distinct from strongly correlated variables. This helps reduce collinearity in the fitting process and prevents the omission of crucial explanatory variables. By considering various correlated parameters, the model not only better characterizes the relationship between independent and dependent variables, improving prediction accuracy, but also detects unusual variations and non-linear relationships, allowing for more precise analysis.

3.3. Model verification

Indicators such as the coefficient of determination (R^2) , absolute error (AE), mean absolute error (MAE), relative error (RE), mean relative error (MRE), and root mean square error (RMSE) were used to assess prediction accuracy. The calculation formulas are shown in Eqs. (7)—(12).

$$R^{2} = 1 - \frac{\sum_{i=1}^{N} \left(IFT_{\exp,i} - IFT_{\text{cal},i} \right)^{2}}{\sum_{i=1}^{N} \left(\overline{IFT}_{\exp,i} - IFT_{\exp,i} \right)^{2}}$$

$$(7)$$

$$AE = IFT_{exp,i} - IFT_{cal,i}$$
 (8)

$$MAE = \frac{1}{N} \sum_{i=1}^{N} \left| IFT_{\exp,i} - IFT_{\text{cal},i} \right|$$
 (9)

$$RE = \frac{IFT_{exp,i} - IFT_{cal,i}}{IFT_{exp,i}} \times 100\%$$
 (10)

$$MRE = \frac{1}{N} \sum_{i=1}^{N} \left(\frac{\left| IFT_{exp,i} - IFT_{cal,i} \right|}{IFT_{exp,i}} \right) \times 100\%$$
 (11)

$$RMSE = \sqrt{\frac{1}{N} \sum_{i=1}^{N} \left(IFT_{exp,i} - IFT_{cal,i}\right)^2}$$
 (12)

where $IFT_{exp,i}$ is the experimental value of the *i*th data point; $IFT_{cal,i}$ is the predicted value of the *i*th data point; and *N* is the number of experimental points.

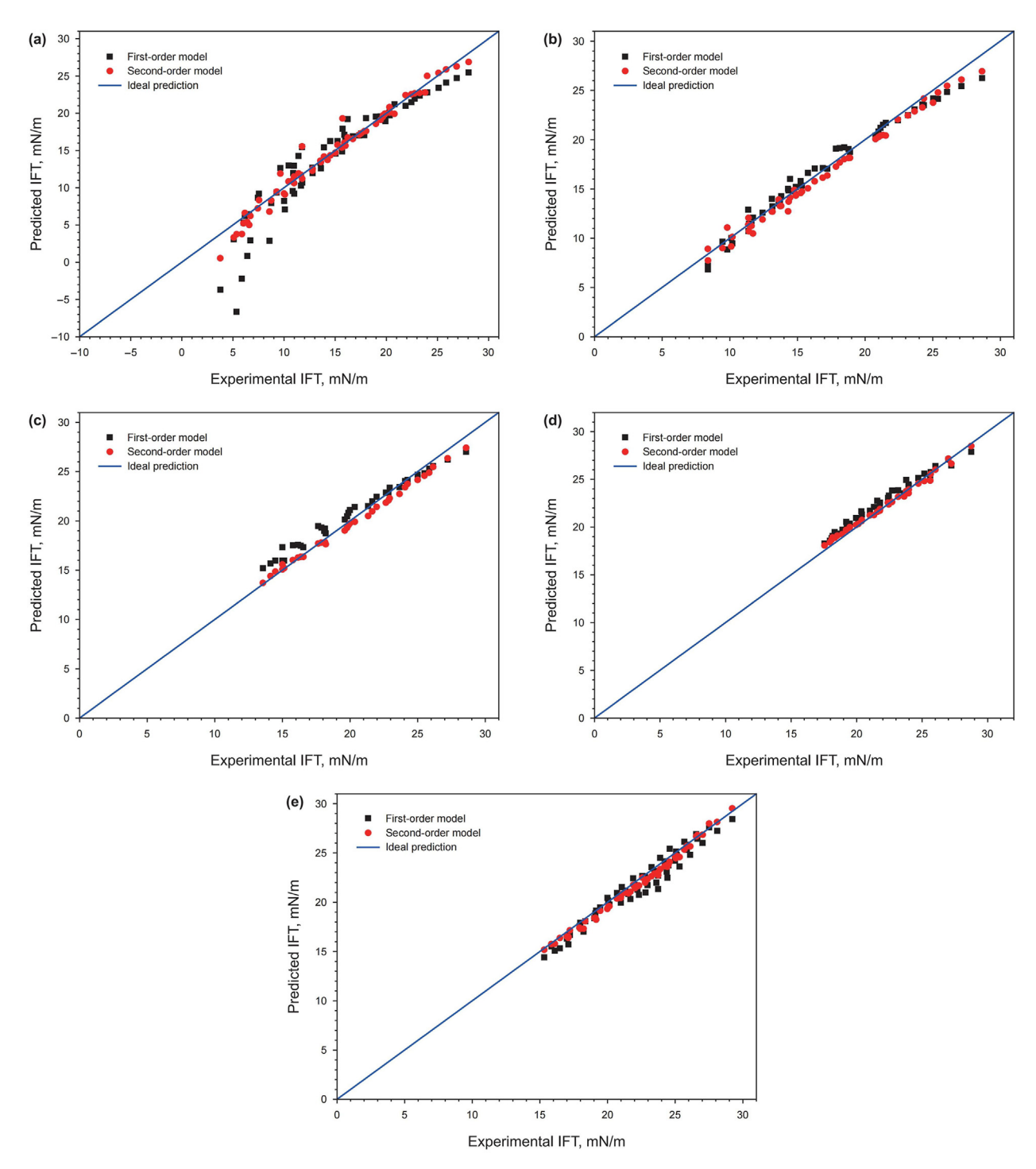


Fig. 5. Comparison of calculated and experimental IFT values in different oil-gas systems. (a) CO₂; (b) CO₂/N₂ (3:1); (c) CO₂/N₂ (1:1); (d) CO₂/N₂ (1:4); (e) N₂.

Fig. 5 compares the calculated and experimental IFT values. The first-order model, which considers only the linear relationship between eight parameters and IFT, shows significant deviation from the experimental values. In contrast, the second-order model, which accounting for linear, quadratic, and synergistic effects, performs better. As shown in Fig. 6, the absolute error of the second-order model is mostly within ± 2 mN/m, and the relative error is generally within $\pm 7\%$. Table 3 compares the calculated and experimental values. The MAE, MRE, and RMSE for the entire dataset are

0.544 mN/m, 3.915%, and 0.739 mN/m, respectively. However, the prediction accuracy of the model decreases with higher CO $_2$ content. While the prediction is accurate when the IFT of the CO $_2$ —crude oil system exceeds 5 mN/m, it worsens in the low IFT region. This is likely due to the aggregation of resin and asphaltene in heavy oil, which inhibits CO $_2$ extraction and prevents low IFT formation. Additionally, low IFT data for conventional light crude oil and CO $_2$ are introduced in this work, which also affect the prediction of CO $_2$ —heavy oil IFT under high pressures.

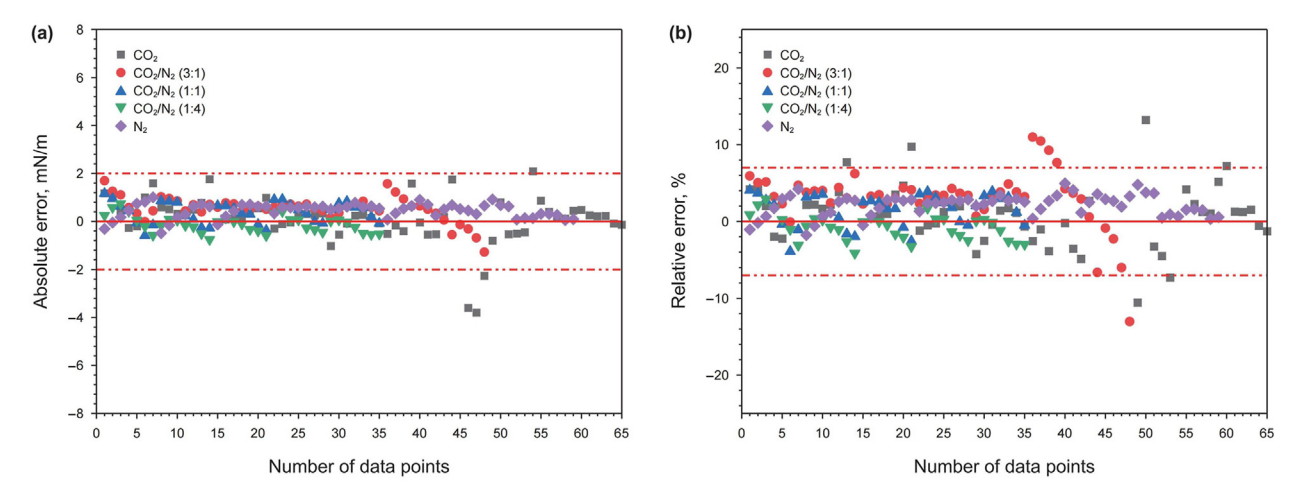


Fig. 6. Distribution of prediction errors for IFT in different oil—gas systems. (a) Absolute error; (b) relative error.

Table 3Statistical analysis of second-order IFT models for different gas systems.

Gas type	N	R^2	MAE, mN/m	MRE, %	RMSE, mN/m
CO ₂	65	0.97419	0.67853	7.47377	1.05232
CO_2/N_2 (3:1)	48	0.99235	0.66185	4.18429	0.74709
CO_2/N_2 (1:1)	35	0.99763	0.49231	2.28922	0.57859
CO_2/N_2 (1:4)	35	0.99467	0.29283	1.41353	0.36540
N ₂	59	0.99287	0.48076	2.22251	0.53693
Total	242	0.98565	0.54429	3.91473	0.73902

4. Results and discussion

4.1. Density difference between saturated oil and gas

Fig. 7 illustrates the density difference between oil and gas under different conditions, with the fitting formula provided in Table S2 of the Supporting Information. At low pressures, the density difference shows minimal variation. However, at higher pressures, it decreases rapidly in oil—gas systems containing CO₂, with the decrease becoming more pronounced as the CO2 concentration increases and the temperature decreases. Lowtemperature, high-pressure conditions favor CO₂ liquefaction. As pressure increases, CO₂ transitions into a high-density state, enhancing its solubility in crude oil. The density difference between oil and gas significantly impacts IFT. Several studies have analyzed its effect based on density variation patterns (Gajbhiye, 2020; Ibrahim et al., 2022; Li et al., 2017; Zhang et al., 2018). Due to limited experimental data, the abnormal density difference behavior under different conditions and its effect on IFT have not been defined or explained.

Temperature affects the density difference between oil and gas in a non-monotonic manner, which can be categorized into two pressure intervals: low-pressure and high-pressure. The transition region is defined as the equivalent density pressure interval (EDPI), where the oil—gas density difference remains unaffected by temperature. EDPI characterizes the effect of temperature on the density difference between oil and gas at varying pressures. In three of the five gas systems, EDPI increased as the CO_2 proportion decreased (Fig. 7(a)—(c)). In Fig. 7(d) and (e), the trend of EDPI formation under higher pressures was observed. As shown in Table S1 of the Supporting Information, at 2 MPa and 60 °C, raising the temperature to 80 °C causes a 0.0130 g/mL decrease in oil phase density, while the gas phase density decreases by only 0.0024 g/mL,

as CO2 has not yet reached the supercritical state. Elevated temperatures expand intermolecular spacing, causing both gas and liquid phases to expand (Yang Z.H. et al., 2015; Yang Y.F. et al., 2023). During this interval, the reduction in oil density is more pronounced than the gas density reduction, and the oil-gas density difference decreases with the increase in temperature. However, at 14 MPa, when the temperature is increased to 80 $^{\circ}$ C, the oil phase density decreases by 0.0085 g/mL, while the CO₂ density decreases by 0.1780 g/mL. This indicates that CO₂, due to its high-density characteristics, is more sensitive to temperature changes. EDPI is more easily observed at lower pressures. When the pressure exceeds EDPI, further increasing in pressure causes the gas to liquefy, significantly increasing gas phase density. In this pressure range, an increase in temperature expands both the intermolecular distance in the gas phase and the liquid phase, but the expansion of the gas phase is more pronounced. The gas density is more sensitive to temperature changes, so the oil-gas density difference becomes more pronounced with the increase in temperature. N₂ can also enter the supercritical state at −147.05 °C and 3.39 MPa. However, its density is much lower than that of pure CO2, making it more difficult for N2 to reach a high-density state under the same pressure (only 0.1362 g/mL at 60 °C and 14 MPa). Additionally, pure N₂ is much less temperature-sensitive than pure CO2. When CO2 and N₂ are mixed in different molar ratios, the gas density decreases as the N₂ concentration increases, which weaken the liquid properties of the gas phase and leads to an increase in EDPI. Even though EDPI does not appear in oil and gas systems with N2 concentrations above 80% at 14 MPa, the curve trend suggests it may occur under higher pressure. As the EDPI increases, the gas compressibility becomes more difficult. To improve oil-gas miscibility, reducing EDPI by increasing CO₂ concentration in the gas phase is a potential solution.

4.2. The influence of pressure

IFT is the force per unit length acting along the interface, caused by the imbalance of forces on the molecules at the interface. As pressure increases, IFT gradually decreases, inversely proportional to pressure (Michaels and Hauser, 1951). As shown in Fig. 8, increasing pressure alters the shape and distribution of the oil—gas interface, causing gas-phase molecules to arrange more closely near the interface. This reduces the distance between oil-phase and gas-phase molecules. As a result, the oil—gas interface thickens, and the droplets transition from rounded to elongated, reducing IFT

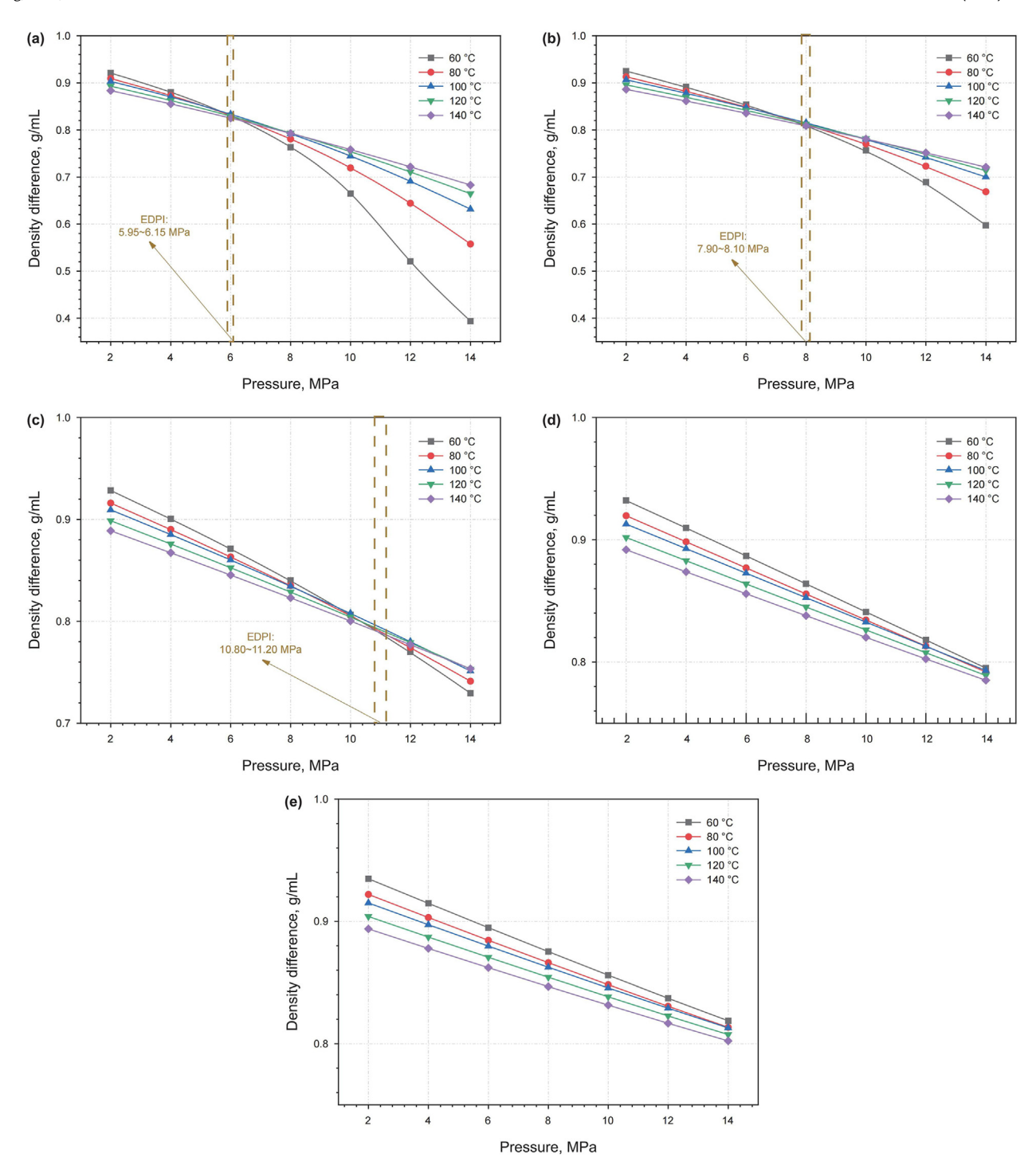


Fig. 7. Density differences between oil and gas under different temperatures, pressures, and gas components. (a) CO₂; (b) CO₂/N₂ (3:1; (c) CO₂/N₂ (1:1); (d) CO₂/N₂ (1:4); (e) N₂.

(Akutsu et al., 2007; Soleimani et al., 2013; Lecacheux et al., 2022). Pressure also significantly impacts mass transfer and solubility at the oil—gas interface. According to Fick's diffusion law (Eq. (13)), the amount of diffusion is directly proportional to the concentration difference at the interface. As the pressure increases, the gas density rises, enhancing the concentration gradient at the oil—gas interface. This leads to an increase in the collision frequency between oil and gas molecules and accelerates the diffusion rate of oil droplets per unit area. Consequently, gas molecules permeate the oil phase more quickly, leading to greater dissolution (Ayirala and

Rao, 2006; Primel et al., 2017), improving the miscibility of oil and gas while further reducing IFT.

$$J = -D\frac{\mathrm{d}C}{\mathrm{d}x} \tag{13}$$

where J is the diffusion flux, kmol/m²·s; D represents the diffusion coefficient, m²/s; C denotes the concentration, kmol/m³; x is the distance in the direction of diffusion, m. This indicates that the diffusion amount of a substance through a unit area per unit time is proportional to the concentration gradient in that area.

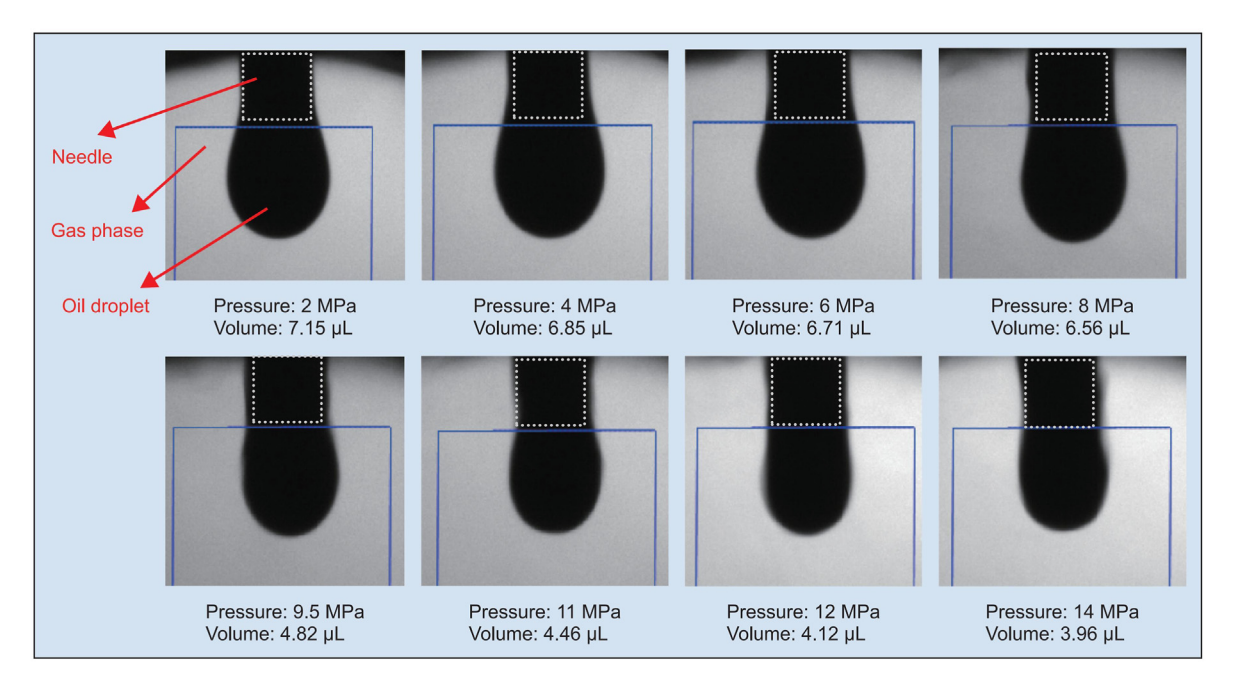


Fig. 8. Oil droplet volume under different pressures in CO2 gas condition.

Extensive research on the IFT-pressure curve has been conducted by numerous scholars, including studies of linear IFT (Li et al., 2017, 2019), two-stage IFT (Wang et al., 2010; Zolghadr et al., 2013b; Zhang et al., 2020), and three-stage IFT (Li et al., 2019; Wang et al., 2010). As shown in Fig. 2, the IFT-pressure curves vary linearly under high temperature or high N₂ content conditions. However, as pressure and CO₂ proportion increase and temperature decreases, distinct inflection points appear on the IFT-pressure curves. These inflection points divide the downward trend of the curves into two stages: one at low pressures and the other at high pressures. At low pressures, IFT decreases rapidly as pressure increases, while at high pressures, the rate of decrease becomes less pronounced. This is caused by the accumulation of lighter components at the oil-gas interface under low pressures, which facilitates the dissolution of CO2. During this stage, the IFT decreases significantly. However, under high pressures, heavier components begin to accumulate at the interface, creating a noticeable polarity difference between CO_2 and the interface colloid, which results in a reduced rate of IFT decrease (Zhang et al., 2024a). Consequently, two pressure intervals were observed, with the pressure corresponding to the inflection point referred to as the minimum equilibrium interfacial tension pressure (Nobakht et al., 2008). The inflection point pressure directly reflects the polarity difference between the gas and oil phases. The IFT γ_n of oil and gas with n components can be divided into the dispersion force contribution $\gamma_n^{\rm d}$ and the polarity force contribution $\gamma_n^{\rm p}$ of the internal molecules to the surface molecules of the oil droplet (Fabien et al., 2022), as shown in Eq. (14).

$$\gamma_n = \gamma_n^d + \gamma_n^p \tag{14}$$

where γ_n represents the oil—gas IFT, mN/m; $\gamma_n^{\rm d}$ denotes the dispersion force contribution, mN/m; and $\gamma_n^{\rm p}$ denotes the polarity force contribution, mN/m.

An increase in temperature or N_2 molar ratio weakens the contributions of dispersion and polarity, causing the inflection point pressure to gradually increase and the IFT to continue rising, which shifts the IFT—pressure diagram to the upper right. At low

pressures, the dispersion contribution dominates. however, as the pressure increases, the net attraction between internal molecules and surface molecules is disrupted, leading to a rapid decrease in IFT. As the pressure continues to rise and reaches the minimum equilibrium interfacial tension pressure, the polarity contribution becomes dominant. Further pressure increases have a weaker effect on enhancing the polarity of both the oil and gas phases, resulting in a slower decrease in IFT.

The IFT cloud maps are shown in Fig. 9. It was observed that the relationship between low IFT and temperature, as well as CO₂ molar proportion, varied under different pressures. As the pressure increased, the low IFT region shifted from the high-temperature area to the low-temperature, high-pressure area. At 2 MPa, where the low IFT region was in the high-temperature area, the increase in temperature can reduce IFT. At 4 MPa, the low IFT region is transferred to high-temperature and high-CO2 areas, where both temperature and gas composition jointly influenced IFT. For every 10 °C rise in temperature or an 18% increase in CO₂ molar proportion, IFT decreases by 0.78 mN/m. When the pressure reached 6 MPa, CO₂ began to liquefy, enhancing the oil-gas interface effect and shifting the low IFT region to areas with higher CO2 content. The CO2 proportion then became the main factor affecting IFT. Above 8 MPa, the low IFT region remained in the low-temperature, high-CO₂ areas. Additionally, the IFT contour distribution also varied with pressure: below 6 MPa, the contours were relatively uniform, while above 6 MPa, they became more scattered. Fig. 9(c)-(g) shows an IFT region unaffected by temperature, where the corresponding CO₂ proportion gradually decreased with increasing pressure, and the average IFT also decreased.

4.3. The influence of temperature

As shown in Fig. 2(a)—(e), temperature did not have a monotonic effect on IFT in systems with a high CO₂ proportion. Temperature variations caused IFT to decrease and increase in distinct pressure intervals. Under low-pressure conditions, temperature disrupts the intermolecular cohesion of oil droplets, decreasing IFT as temperature increases. Under high-pressure conditions,

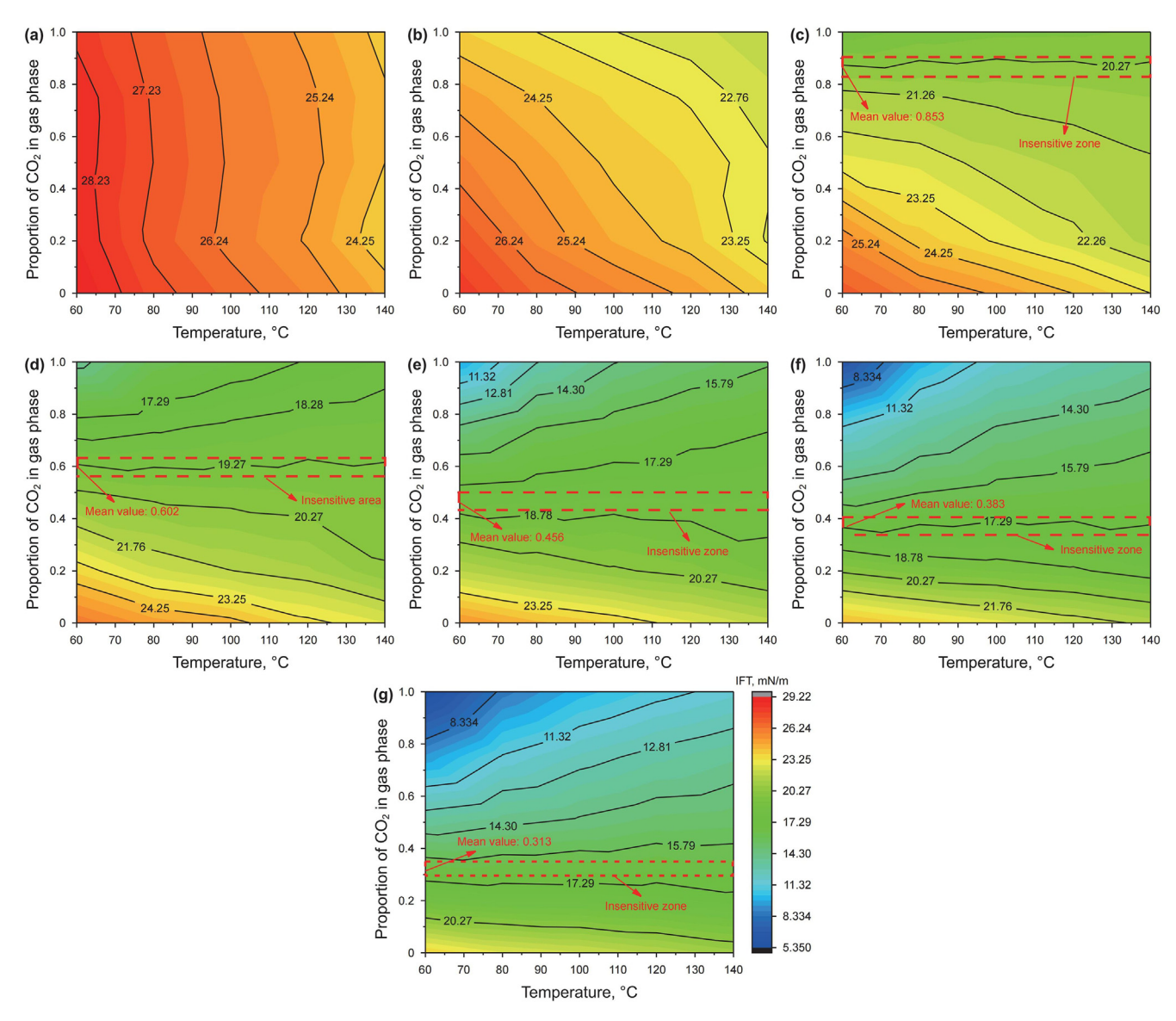


Fig. 9. Cloud maps of IFT at different pressure conditions. (a) 2 MPa; (b) 4 MPa; (c) 6 MPa; (d) 8 MPa; (e) 10 MPa; (f) 12 MPa; (g) 14 MPa.

temperature disrupts the high-density characteristics of CO₂, causing IFT to increase with temperature. When CO₂ proportion was low, temperature had a more direct effect on IFT. Within the experimental pressure range, IFT decreased linearly with temperature increasing, and the absolute value of the fitting slope decreased, leading to a smaller reduction in IFT per unit pressure (Zolghadr et al., 2013a). A lower CO₂ proportion resulted in a smaller effect of temperature increase on the gas phase but a greater effect on the oil phase. Although increasing temperature helped reduce the IFT between oil and gas, its effectiveness was limited by considerable polarity differences. Additionally, the solubility of gas in crude oil decreases as temperature increases (Ghorbani and Mohammadi, 2017; Mutailipu et al., 2024). According to Henry's law, higher temperatures affect the equilibrium between gas and oil droplets. Increased molecular movement within the oil droplet creates more intermolecular space, reducing the effective contact area and time for gas molecules in the oil phase. This promotes the separation of gas molecules from the oil phase. decreasing oil-gas miscibility and increasing IFT.

Fig. 10 illustrates the cloud map of oil—gas IFT distribution under various temperature conditions. At all temperature, the low IFT region is consistently located in areas of high pressure and high CO₂ proportion, with temperature fluctuations having a minimal effect on the IFT distribution pattern. Moreover, a larger reduction in IFT under high-temperature and high-pressure conditions can only be achieved by lowering the temperature or increasing the CO₂ proportion. For instance, when the temperature decreased from 140 to 60 °C, IFT dropped from 11.65 to 5.30 mN/m. Similarly, when the CO₂ proportion increased from 0 to 1 (molar ratio increased from 0 to 100%), IFT decreased from 20.99 to 11.65 mN/m. The study found that reducing the temperature is more effective in promoting low IFT formation under high temperature and pressure conditions, as it enhances the supercritical properties of CO₂, improving its interaction with oil and gas phases. Additionally, under lowtemperature and high-pressure conditions, increasing the CO₂ ratio is more effective, enhancing the mutual solubility between the oil and gas phases, and leading to a greater reduction in IFT.

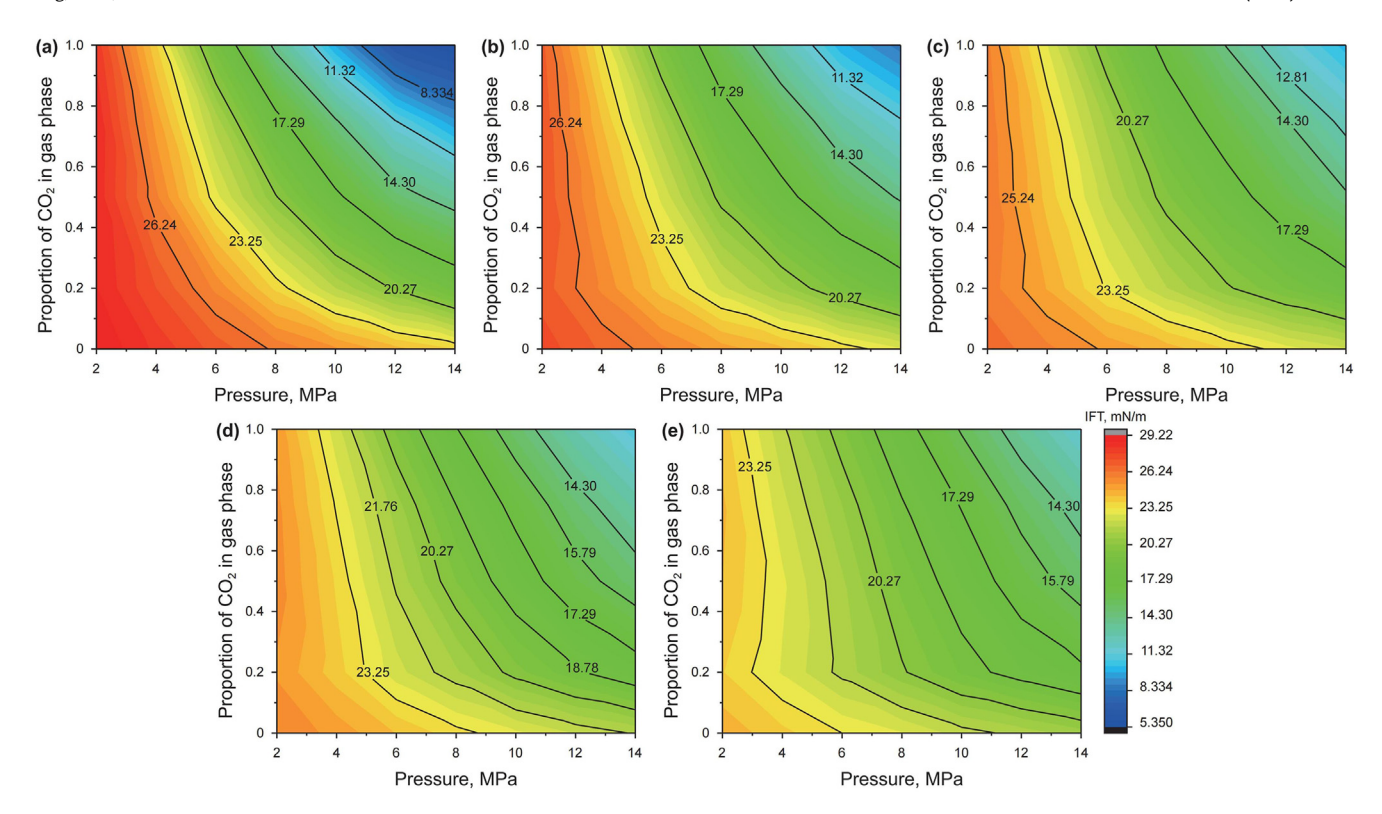


Fig. 10. Cloud maps of IFT at different temperature conditions. (a) 60 °C; (b) 80 °C; (c) 100 °C; (d) 120 °C; (e) 140 °C.

4.4. The influence of gas composition

According to Fig. S2 of the Supporting Information, the IFT of various oil and gas systems showed minimal variation at low pressures. However, at high pressures, IFT decreased in the following order: pure CO₂, CO₂/N₂ (3:1), CO₂/N₂ (1:1), CO₂/N₂ (1:4), and pure N2. In the immiscible phase state, small CO2 bubbles dispersed in crude oil, with some capacity for expansion. This caused oil volume expansion, which reduced oil density and IFT. N₂, a common inert gas, has 1/5 to 1/10 of the solubility of CO₂ in crude oil under high pressures (Su et al., 2023). Due to its poor miscibility and low solubility in crude oil, N2 had a limited effect on IFT compared to CO₂. The effects of different CO₂/N₂ ratios on IFT were intermediate between CO2 and N2. Experimental results showed that increasing the CO₂ proportion in the gas phase decreased oil-gas IFT, while increasing N₂ proportion increased it. With a higher CO₂ proportion, its high solubility weakened the strength of intermolecular interactions within oil droplets (Sevyedattar et al., 2023), thereby reducing IFT. At low-temperature and lowpressure conditions, oil-gas IFT reaches its maximum value. Increasing either temperature or pressure can reduce IFT. Due to the significant density difference between oil and gas at low pressures, increasing the CO₂ proportion has a minimal impact on IFT. Conversely, under low-temperature and high-pressure conditions, IFT is minimized. To further reduce IFT, increasing pressure or enhancing the CO₂ proportion is effective. Under high-temperature and low-pressure conditions, increasing the CO2 proportion or temperature slightly reduces IFT, while increasing pressure is more effective. At high pressures, both increasing the CO₂ proportion and decreasing temperature reduce IFT, but when CO₂ proportion is already high, reducing temperature is preferred.

Fig. 11 illustrates the oil—gas IFT distribution cloud maps at various CO₂/N₂ ratios. At lower CO₂ ratios, the minimum IFT of 20.99 mN/m occurred under high-temperature and high-pressure

conditions. As the CO_2 ratio increases, IFT decreases progressively, reaching minimum values of 17.55, 13.56, 9.45, and 5.23 mN/m, all within high-pressure regions. However, the temperature selectivity of the low IFT region is not unique and is primarily influenced by the gas composition. As the CO_2 ratios increase, low IFT regions shift from high-temperature to low-temperature zones, consistent with CO_2 's temperature sensitivity. It was found that at lower CO_2 ratios, IFT can be reduced by increasing temperature or pressure. In contrast, at higher CO_2 ratios, IFT is reduced by increasing pressure or lowering temperature.

A non-linear increase in oil-gas IFT reduction was observed between 2 and 14 MPa as the CO₂ proportion increased. As shown in Fig. 12, at 60 °C, IFT decreased by 0.24 mN/m for each 1% increase in CO₂ molar proportion from 0 to 20%. When the CO₂ proportion reached 50%, IFT decreased by 0.16 mN/m for each additional 1% increase in the range of 20%–50%. The increase in CO₂ proportion did not lead to a significant further reduction in IFT, with the reduction effect gradually weakening, especially under high-temperature conditions. At low temperature, the density difference is small, and the interaction at the two-phase interface is strong. At elevated temperatures, the significant decrease in supercritical CO₂ density and the greater distance between oil and gas molecules weaken the interface effect. This phenomenon is also influenced by "competitive dissolution" of CO₂/N₂ in crude oil. Competitive dissolution refers to the competition between solute and solvent in a solution. While much research has been conducted on competitive dissolution in solid-liquid systems (Hári et al., 2016; Seyeux et al., 2008), fewer studies have been conducted on gas-liquid systems. Due to instrumental limitations, it is challenging to capture the extent of different gas dissolution in the liquid phase under high pressure. Therefore, quantitatively characterizing the dissolution behavior of CO₂/N₂ in crude oil is difficult, and only limited analysis can be performed based on the polarity differences between the two phases. When CO₂ and N₂ are introduced into crude oil, they compete

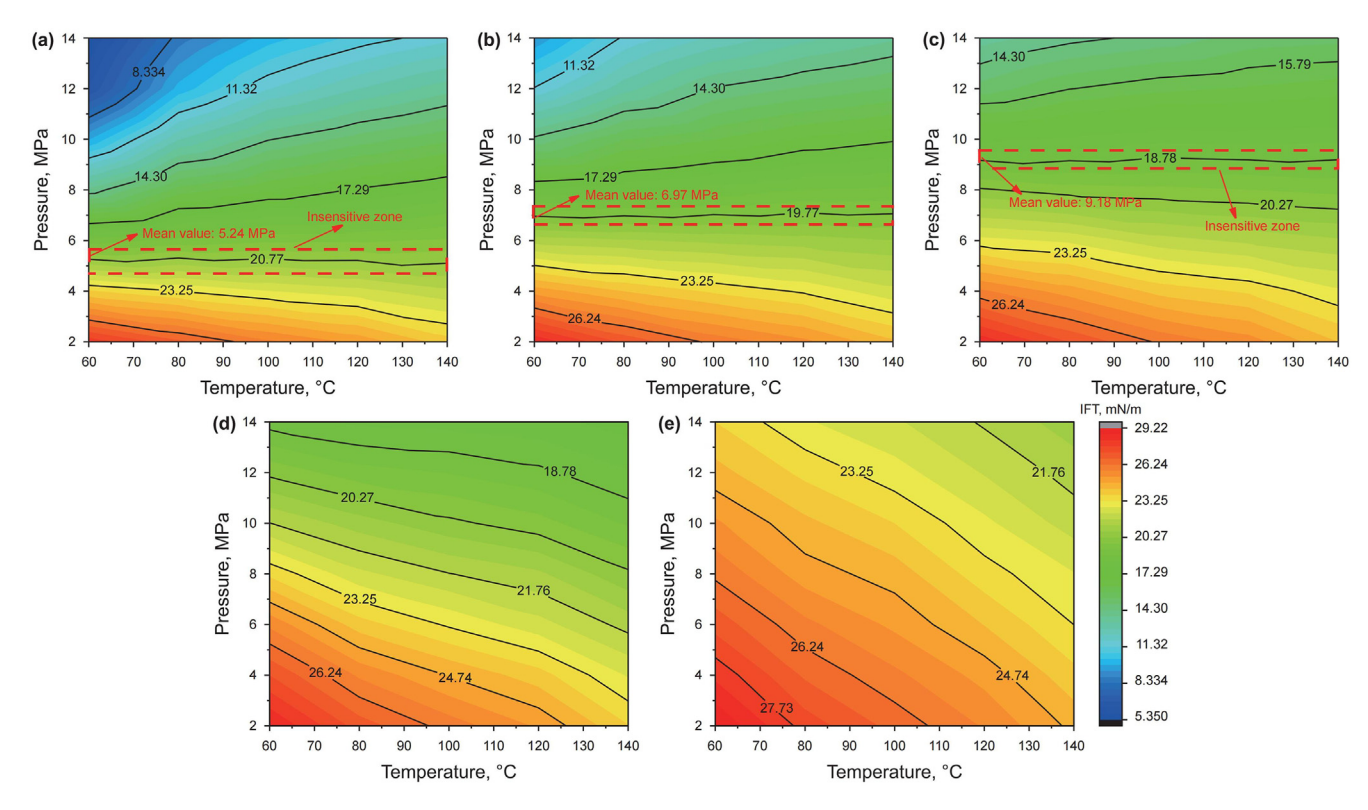


Fig. 11. Cloud maps of IFT at different gas composition conditions. (a) CO₂; (b) CO₂/N₂ (3:1); (c) CO₂/N₂ (1:1); (d) CO₂/N₂ (1:4); (e) N₂.

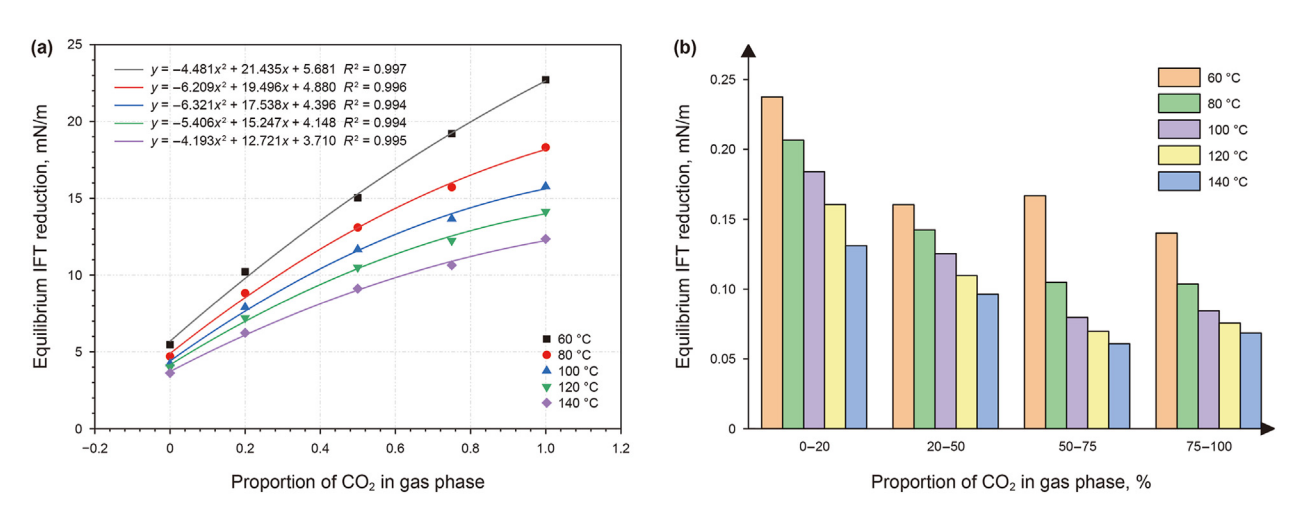


Fig. 12. Effect of CO₂ ratio on IFT. (a) IFT reduction within the range of 2–14 MPa under different temperature and gas composition conditions; (b) IFT reduction for each 1% increase in molar proportion of CO₂ in the gas phase.

for dissolution. CO_2 , with higher solubility, dissolves more readily in crude oil, while N_2 , with lower solubility, dissolves less. When CO_2/N_2 with a molar ratio of 1:4 is injected, the higher solubility of CO_2 in crude oil likely causes the ratio of CO_2/N_2 dissolved in the oil to exceed the injected gas ratio, leading to oil expansion and improving droplet shape, resulting in a rapid reduction in IFT. However, further increases in CO_2 proportion lead to diminished dissolution effects due to limited solubility, limiting droplet shape improvement and weakening the ability to reduce IFT. At low temperatures, gas solubility in crude oil is higher, and increasing the CO_2 proportion leads to the continuous dissolution of CO_2 and a decrease in IFT. At high temperatures, gas solubility is lower, and injecting a small amount of CO_2/N_2 gas allows a higher proportion of CO_2 to dissolve in the oil,

limiting the ability to reduce IFT by increasing CO_2 content. From an engineering perspective, increasing the CO_2 proportion in injected gas can quickly reduce IFT and improve oil displacement in low-temperature reservoirs. In high-temperature reservoirs or CO_2/N_2 -assisted steam huff and puff processes, the optimal approach is to inject a specific ratio of CO_2/N_2 to minimize CO_2 capture costs, enhance reservoir energy, and prevent IFT anomalies due to temperature increases.

4.5. The influence of EITP

Oil—gas IFT is significantly affected by external conditions. Experimental results show that IFT has a monotonic relationship

with pressure and CO₂/N₂ ratio, while the effect of temperature on IFT is characterized by two distinct regions. As discussed previously, this phenomenon is primarily due to the significant effect of temperature on the CO₂ phase at high pressures, resulting in the emergence of EDPI. Since the density difference is a key parameter for IFT, there exists a pressure range where IFT is insensitive to temperature changes. As shown in Fig. 9(c)–(g) and Fig. 11(a)–(c), eight slices demonstrate an IFT range that is nearly unaffected by temperature variations, although this range is relatively narrow. Extensive experimental validation is needed to confirm whether this region can be represented by an average pressure point for simplification. The average pressure points and CO₂/N₂ ratios of each insensitive zone in these slices were selected for temperature rise experiments, with a temperature range of 60-140 °C, at an interval of 10 °C. As shown in Fig. S3 of the Supporting Information, under the eight different pressure and gas ratio conditions, IFT exhibited disorder with increasing temperature but was largely unaffected by temperature. Table S3 (Supporting Information) indicates that the maximum relative error between the upper and lower boundaries and the average value are 1.17% and 0.943%, respectively, with the overall average relative error being under 0.5%. Therefore, this narrow interval can be represented by a single pressure point. In this study, the pressure corresponding to the insensitive zone in different slices is defined as the "equivalent interfacial tension pressure during temperature change (EITP)", which refers to a pressure in the same oil and gas system that makes IFT equal at different temperatures.

Some scholars have conducted CO₂—oil interfacial tension tests and found that IFT decreases with increasing temperature at low pressures, but this trend reverses at higher pressures for all systems studied (Zolghadr et al., 2013a; Li et al., 2017; Ibrahim et al., 2022). Shang et al. (2017) tested IFT for CO₂/N₂ and paraffin and found that IFT exhibits the weakest temperature dependence at the crossover pressure. To maintain optimal conditions, CO2 should be injected at a lower temperature above the crossover pressure and at a higher temperature below it. However, due to limited experimental data, this phenomenon has not been fully defined or analyzed in terms of oil and gas properties. Flue gas injection is an effective method for developing heavy oil reservoirs. To maintain formation pressure and enhance oil recovery, co-injecting CO₂/N₂ with steam is essential. During multi-component thermal fluid injection, thermal energy propagates from the near-wellbore region to deeper oil formations. Accurately determining the interface parameters of different CO₂/ N₂—heavy oil systems and how they vary with temperature changes is crucial for improving heavy oil thermal recovery. Building on previous work, this study conducted oil-gas IFT experiments and observed equivalent IFT in different CO₂/N₂-oil systems, defining the pressure at which equivalent IFT occurs during temperature changes as EITP (equivalent interfacial tension pressure). On the EITP curve, temperature changes have little effect on oil-gas IFT. A higher EITP indicates a weaker ability of injected gas to reduce IFT. When the pressure is below the EITP, IFT decreases as temperature increases. Temperature has a greater effect on the oil phase than gas composition. Rising temperatures disrupt the cohesion among crude oil molecules, intensifying thermal motion and weakening attraction between molecules in the oil droplet and those at its interface, reducing the density difference between oil and gas and IFT. When pressure exceeds EITP, IFT increases with rising temperature, with the gas phase being more sensitive to temperature changes than the liquid phase. Under high pressures, CO2 enters a high-density stage, increasing the gas phase sensitivity to temperature, increasing the distance between oil and gas molecules, and rapidly increasing the density difference. From Fig. 13, as the CO₂ proportion decreases, EITP decreases non-linearly but gradually slows down. Despite the significant impact of density difference on IFT, EITP is consistently

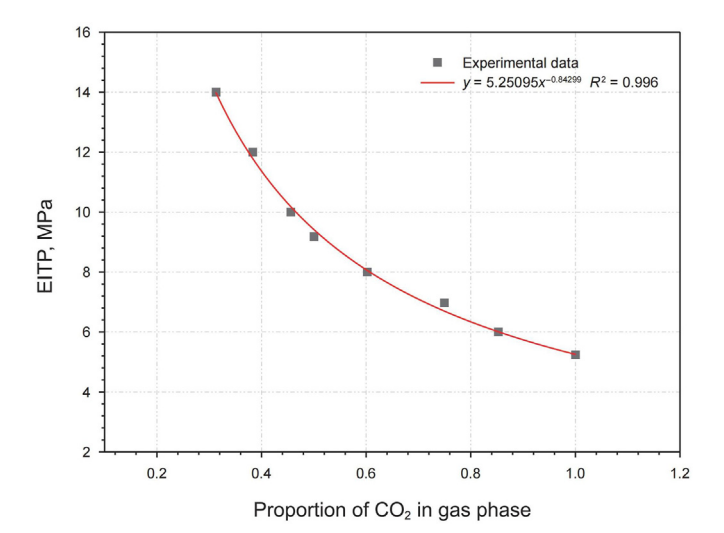


Fig. 13. Effect of CO₂/N₂ ratio on EITP.

lower than EDPI (Fig. 7). According to Eq. (1), IFT is influenced not only by the density difference but also by parameters like the curvature radius of oil droplets and the running angle. At the same density difference and pressure, lower temperature corresponds to smaller IFT, enhancing oil—gas interaction, increasing solubility, and reducing IFT.

In CO₂/N₂-assisted steam huff and puff operations, the bottom hole injection temperature of the thermal fluid ranges from 250 to 350 °C. Upon entering the reservoir, the thermal fluid primarily transfers heat through thermal convection to the distant well area. Over time, the frontier edge steam gradually condenses, and the average temperature within the fluid heating radius stabilizes at 150–250 °C. The introduction of CO₂/N₂ not only improves steam quality and helps carry heat to the top of the reservoir, forming a heat-insulating layer that reduces steam heat loss to the upper layer, but also replenishes formation energy to maintain oil production (Dong et al., 2019). Minimizing the negative impact of high temperatures on oil-gas IFT is crucial in this process. CO₂/N₂ mixtures can enhance oil recovery and facilitate carbon sequestration. Our recent study explored the effect of N2 as an impurity gas on CO2 storage performance, highlighting the safety and sustainability of CO₂ storage from the perspective of gas-liquid-solid interactions. N₂ addition creates dissolution pits on calcite surfaces, and the calcite matrix exhibits optimal water-wettability at 50%-75% CO₂ enrichment, which increases CO₂ storage column heights (Zhang et al., 2024b). Regarding enhanced oil recovery (EOR), it is often believed that higher CO2 injection ratios improve EOR efficiency; however, this is not true for heavy oil reservoirs. Excessive CO₂ can extract residual oil in the reservoir, deteriorating its physical properties and forming an oil barrier, which reducing the effectiveness of later-stage oil and gas production. A certain amount of N₂ in CO₂ can improve crude oil production efficiency in porous media. Currently, CO₂/N₂ injection ratios are determined through laboratory core displacement experiments (Wang et al., 2021; Li et al., 2022), but this method does not fully reveal the impact of different CO₂/N₂ ratios on oil-gas interface properties. The EITP curve for the CO₂/N₂ system illustrates the effect of temperature variations on IFT under different gas ratios. EITP is the critical boundary where oil-gas IFT is affected by temperature; above this boundary, IFT increases with temperature. Injecting more CO₂ does not rapidly reduce IFT but results in CO₂ waste. High temperature and CO2 extraction of heavy oil also cause the loss of light components, degrading physical properties of the remaining oil and

complicating subsequent development. For example, in the Zheng364 block oil reservoir in the Shengli Oilfield, located at a depth of 1175 m with a formation pressure of 11 MPa and a temperature of 60 °C, the optimal CO_2/N_2 ratio was determined to be 0.4064 based on the EITP curve. At this ratio, injecting hot gas prevents excessive extraction of crude oil, avoiding the loss of light and medium components while ensuring that temperature changes do not adversely affect IFT.

5. Conclusions

In this study, oil—gas IFT was measured under various conditions using the pendant drop technique. A reliable model was developed to predict the oil—gas IFT based on temperature, pressure, and CO_2/N_2 ratio. A 3D IFT model was created, and 2D cloud maps were plotted under constant temperature, pressure, and CO_2 proportion to analyze IFT variation patterns and influencing mechanisms. The findings are as follows:

- (1) IFT shows a strong correlation with oil—gas density difference, a moderate correlation with pressure and CO₂ proportion, a weak correlation with saturates content and resin content, and a nonlinear correlation with temperature, aromatics content, and asphaltene content. After data expansion, the combination of linear, quadratic, and synergistic effects accurately characterizes the relationship between independent and dependent variables, detecting abnormal changes and nonlinear trends in the data set, leading to more accurate predictions.
- (2) As pressure increases, the low IFT region shifts from the high-temperature area to the low-temperature, high-CO₂ content region. Under low pressures, the influence of temperature on IFT is dominant, while under high pressures, the influence of CO₂ proportion on IFT is dominant.
- (3) The pressure corresponding to the equivalent IFT during temperature changes is defined as EITP, which divides the effect of temperature on IFT into two pressure intervals. At specific pressures and CO_2/N_2 ratios, temperature increases have little effect on IFT.
- (4) The competitive dissolution of CO_2/N_2 in crude oil and the reduced gas solubility in the system at high temperatures lead to a nonlinear increase in IFT reduction as the CO_2 proportion increases. At high temperatures, a low CO_2/N_2 ratio achieves the most economical reduction in IFT.
- (5) In engineering applications, when reservoir pressure is low, increasing the CO₂ ratio has minimal impact on IFT. Raising the reservoir temperature can reduce IFT to some extent, but the effect is limited. When the reservoir pressure is high, increasing the CO₂ ratio at low temperatures can rapidly reduce IFT. At high temperatures or during gas-assisted steam huff and puff, it is best to lower the system temperature or determine the optimal CO₂/N₂ injection ratio using the EITP curve.

CRediT authorship contribution statement

Chao Zhang: Writing — review & editing, Supervision, Project administration, Methodology. **Chao Yu:** Writing — original draft, Methodology, Investigation, Data curation. **Zi-Han Gu:** Methodology, Formal analysis, Data curation. **Kun Liu:** Visualization, Software, Data curation. **Ping-Keng Wu:** Visualization, Supervision, Methodology. **Zhao-Min Li:** Writing — review & editing, Supervision, Methodology.

Declaration of competing interest

The authors declare that they have no known competing financial interests or personal relationships that could have appeared to influence the work reported in this paper.

Acknowledgements

This work was supported by National Natural Science Foundation of China (52204068 and U20B6003), and the Program for Scientific Research Innovation Team of Young Scholars in Colleges and Universities of Shandong Province (2022KJ067). We are grateful to the Shandong Engineering Research Center of Carbon Dioxide Utilization and Storage for the assistance with our experimental research. The valuable comments made by the anonymous reviewers are also sincerely appreciated.

Appendix A. Supplementary data

Supplementary data to this article can be found online at https://doi.org/10.1016/j.petsci.2025.03.032.

References

- Abedini, A., Torabi, F., 2014. Oil recovery performance of immiscible and miscible CO₂ huff-and-puff processes. Energy Fuels 28 (2), 774–784. https://doi.org/10.1021/ef401363b.
- Akutsu, T., Yamaji, Y., Yamaguchi, H., et al., 2007. Interfacial tension between water and high pressure CO₂ in the presence of hydrocarbon surfactants. Fluid Phase Equilib. 257 (2), 163–168. https://doi.org/10.1016/j.fluid.2007.01.040.
- Alvarado, V., Manríque, E., 2010. Enhanced oil recovery: an update review. Energies 3 (9), 1529–1575. https://doi.org/10.3390/en3091529.
- Amidror, I., 2002. Scattered data interpolation methods for electronic imaging systems: a survey. J. Electron. Imag. 11 (2), 157–176. https://doi.org/10.1117/1.1455013.
- Andreas, J.M., Hauser, E.A., Tucker, W.B., 1938. Boundary tension by pendant drops. J. Phys. Chem. 42 (8), 1001–1019. https://doi.org/10.1021/j100903a002.
- Ayirala, S.C., Rao, D.N., 2006. Solubility miscibility and their relation to interfacial tension in ternary liquid systems. Fluid Phase Equilib. 249 (1–2), 82–91. https://doi.org/10.1016/j.fluid.2006.09.020.
- Bera, A., Babadagli, T., 2015. Status of electromagnetic heating for enhanced heavy oil/bitumen recovery and future prospects: a review. Appl. Energy 151, 206–226. https://doi.org/10.1016/j.apenergy.2015.04.031.
- Bautista, E.V., Barillas, J.L.M., Dutra, T.V., et al., 2014. Capillary, viscous and gravity forces in gas-assisted gravity drainage. J. Pet. Sci. Eng. 122, 754–760. https:// doi.org/10.1016/j.petrol.2014.09.018.
- Bender, S., Akin, S., 2017. Flue gas injection for EOR and sequestration: case study. J. Pet. Sci. Eng. 157, 1093–1105. https://doi.org/10.1016/j.petrol.2017.07.044.
- Bansal, A., Sharma, R., Kathuria, M., 2022. A systematic review on data scarcity problem in deep learning: solution and applications. ACM Comput. Surv. 54 (10S), 208. https://doi.org/10.1145/3502287.
- Behvandi, R., Mirzaie, M., 2022. A novel correlation for modeling interfacial tension in binary mixtures of CH₄, CO₂ and N₂ + normal alkanes systems: application to gas injection EOR process. Fuel 325, 124622. https://doi.org/10.1016/ifuel_2022.124622.
- Chen, H., Liu, X.L., Zhang, C., et al., 2022. Effects of miscible degree and pore scale on seepage characteristics of unconventional reservoirs fluids due to supercritical CO₂ injection. Energy 239, 122287. https://doi.org/10.1016/j.energy.2021.122287.
- Dong, X.H., Liu, H.Q., Chen, Z.X., et al., 2019. Enhanced oil recovery techniques for heavy oil and oilsands reservoirs after steam injection. Appl. Energy 239, 1190–1211. https://doi.org/10.1016/j.apenergy.2019.01.244.
- Enders, S., Quitzsch, K., 1998. Calculation of interfacial properties of demixed fluids using density gradient theory. Langmuir 14 (16), 4606–4614. https://doi.org/ 10.1021/la9712707.
- Fabien, A., Lefebvre, G., Calvignac, B., et al., 2022. Interfacial tension of ethanol, water, and their mixtures in high pressure carbon dioxide: measurements and modeling. J. Colloid Interface Sci. 613, 847–856. https://doi.org/10.1016/i.icis.2022.01.058.
- Gajbhiye, R., 2020. Effect of CO₂/N₂ mixture composition on interfacial tension of crude oil. ACS Omega 5 (43), 27944–27952. https://doi.org/10.1021/acsomega.0c03326.
- Garcea, F., Serra, A., Lamberti, F., et al., 2023. Data augmentation for medical imaging: a systematic literature review. Comput. Biol. Med. 152, 106391. https://doi.org/10.1016/j.compbiomed.2022.106391.
- Ghorbani, M., Mohammadi, A.H., 2017. Effects of temperature, pressure, and fluid composition on hydrocarbon gas-oil interfacial tension (IFT): an experimental

study using ADSA image analysis of pendant drop test method. J. Mol. Liq. 227, 318–323. https://doi.org/10.1021/ie401283q.

- Hári, J., Gyürki, A., Sárközi, M., et al., 2016. Competitive interactions and controlled release of a natural antioxidant from halloysite nanotubes. J. Colloid Interface Sci. 462, 123–129. https://doi.org/10.1016/j.jcis.2015.09.054.
- Hasanvand, M.Z., Golparvar, A., 2014. A critical review of improved oil recovery by electromagnetic heating. Petrol. Sci. Technol. 32 (6), 631–637. https://doi.org/10.1080/10916466.2011.592896.
- He, X.J., Zhao, L.D., Lu, X.Q., et al., 2022. A critical review using CO₂ and N₂ of enhanced heavy-oil-recovery technologies in China. Appl. Sci. 12 (24), 12585. https://doi.org/10.3390/app122412585.
- Hemmati-Sarapardeh, A., Ayatollahi, S., Ghazanfari, M.H., et al., 2013. Experimental determination of interfacial tension and miscibility of the CO₂—crude oil system; temperature, pressure and composition effects. J. Chem. Eng. Data 59 (1), 61–69. https://doi.org/10.1021/je400811h.
- Hemmati-Sarapardeh, A., Ayatollahi, S., Zolghadr, A., et al., 2014. Experimental determination of equilibrium interfacial tension for nitrogen-crude oil during the gas injection process: the role of temperature, pressure, and composition. I. Chem. Eng. Data 59 (11), 3461–3469. https://doi.org/10.1021/je5004274.
- Hwang, R.J., Ortiz, J., 2000. Mitigation of asphaltics deposition during CO₂ flood by enhancing CO₂ solvency with chemical modifiers. Org. Geochem. 31 (12), 1451–1462. https://doi.org/10.1016/S0146-6380(00)00082-6.
- Ibrahim, A.F., Abdelgawad, K.Z., Al-Anazi, A., et al., 2022. Effect of crude oil properties on the interfacial tension of crude oil/CO₂ under HPHT conditions. Arabian J. Sci. Eng. 48 (7), 9269—9286. https://doi.org/10.1007/s13369-022-07291-6.
- International Energy Agency, 2024. World energy Statistics. Available: https://www.iea.org/data-and-statistics/data-product/world-energy-statistics#energy-statistics. Accessed July 2024.
- Johnsson, F., Kjärstad, J., Rootzén, J., 2019. The threat to climate change mitigation posed by the abundance of fossil fuels. Clim. Policy 19 (2), 258–274. https://doi.org/10.1080/14693062.2018.1483885.
- Kong, S.Q., Feng, G., Liu, Y.L., et al., 2021. Potential of dimethyl ether as an additive in CO₂ for shale oil recovery. Fuel 296, 120643. https://doi.org/10.1016/ i.fuel.2021.120643.
- Lecacheux, L., Sadoudi, A., Duri, A., et al., 2022. The role of laplace pressure in the maximal weight of pendant drops. J. Colloid Interface Sci. 606, 920–928. https://doi.org/10.1016/j.jcis.2021.08.047.
- Leung, D.Y.C., Caramanna, G., Maroto-Valer, M.M., 2014. An overview of current status of carbon dioxide capture and storage technologies. Renew. Sustain. Energy Rev. 39, 426–443. https://doi.org/10.1016/j.rser.2014.07.093.
- Li, H.Z., Yang, D.Y., Tontiwachwuthikul, P., 2012. Experimental and theoretical determination of equilibrium interfacial tension for the solvent(s)-CO₂-heavy oil systems. Energy Fuels 26 (3), 1776–1786. https://doi.org/10.1021/ef201860f.
- Li, N., Zhang, C.W., Ma, Q.L., et al., 2017. Interfacial tension measurement and calculation of (carbon dioxide + *n*-alkane) binary mixtures. J. Chem. Eng. Data 62 (9), 2861–2871. https://doi.org/10.1021/acs.jced.7b00159.
- Li, N., Zhang, C.W., Ma, Q.L., et al., 2019. Measurements and modeling of interfacial tension for (CO₂ + *n*-alkyl benzene) binary mixtures. J. Supercrit. Fluids 154, 104625. https://doi.org/10.1016/j.supflu.2019.104625.
- Li, S.Y., Sun, L., Wang, L., et al., 2022. Hybrid CO₂-N₂ huff-n-puff strategy in unlocking tight oil reservoirs. Fuel 309, 122198. https://doi.org/10.1016/i.fuel.2021.122198.
- Li, Y.B., Pu, W.F., Wei, B., et al., 2018. The feasibility of CO₂ and N₂ injection for the Tahe fracture-cavity carbonate extra-heavy oil reservoir: an experimental study. Fuel 226, 598–606. https://doi.org/10.1016/j.fuel.2018.04.056.
- Liu, X.L., Chen, H., Chen, Z.H., et al., 2024. Study on characterization and distribution of four regions of tight sandstone condensate gas reservoirs in the depletion development process. Fuel 358, 130267. https://doi.org/10.1016/j.fuel.2023.130267.
- Liu, Y.L., Rui, Z.H., 2022. A storage-driven CO₂ EOR for a net-zero emission target. Engineering 18, 79–87. https://doi.org/10.1016/j.eng.2022.02.010.
- Lv, Q.C., Zhou, T.K., Zheng, R., et al., 2023. Application of group method of data handling and gene expression programming for predicting solubility of CO₂-N₂ gas mixture in brine. Fuel 332, 126025. https://doi.org/10.1016/j.fuel.2022.126025.
- Ma, Y., Li, Y., Huang, G., 2023. Planning China's non-deterministic energy system (2021-2060) to achieve carbon neutrality. Appl. Energy 334, 120673. https://doi.org/10.1016/j.apenergy.2023.120673.
- Michaels, A.S., Hauser, E.A., 1951. Interfacial tension at elevated pressure and temperature. II Interfacial properties of hydrocarbon-water systems. J. Phys. Colloid Chem. 55 (3), 408–421. https://doi.org/10.1021/j150486a008.
- Mokheimer, E.M.A., Hamdy, M., Abubakar, Z., et al., 2018. A comprehensive review of thermal enhanced oil recovery: techniques evaluation. J. Energy Resour. Technol. 141 (3), 030801. https://doi.org/10.1115/1.4041096.
- Mutailipu, M., Song, Y.C., Yao, Q., et al., 2024. Solubility and interfacial tension models for CO₂-brine systems under CO₂ geological storage conditions. Fuel 357, 129712. https://doi.org/10.1016/j.fuel.2023.129712.
- Nguyen, P., Carey, J.W., Viswanathan, H.S., et al., 2018. Effectiveness of supercritical-CO₂ and N₂ huff-and-puff methods of enhanced oil recovery in shale fracture networks using microfluidic experiments. Appl. Energy 230, 160–174. https://doi.org/10.1016/j.apenergy.2018.08.098.
- Ni, H., Hsu, C.S., Lee, P., et al., 2015. Supercritical carbon dioxide extraction of petroleum on kieselguhr. Fuel 141, 74—81. https://doi.org/10.1016/j.fuel.2014.09.126.

- Nobakht, M., Moghadam, S., Gu, Y., 2008. Mutual interactions between crude oil and CO₂ under different pressures. Fluid Phase Equilib. 265 (1–2), 94–103. https://doi.org/10.1016/j.fluid.2007.12.009.
- Orr, F.M., Taber, J.J., 1984. Use of carbon dioxide in enhanced oil recovery. Science 224 (4649), 563–569. https://doi.org/10.1126/science.224.4649.563.
- Primel, A., Férec, J., Ausias, G., et al., 2017. Solubility and interfacial tension of thermoplastic polyurethane melt in supercritical carbon dioxide and nitrogen. J. Supercrit. Fluids 122, 52–57. https://doi.org/10.1016/j.supflu.2016.11.016.
- Rezk, M.G., Foroozesh, J., 2018. Determination of mass transfer parameters and swelling factor of CO₂-oil systems at high pressures. Int. J. Heat Mass Tran. 126, 380–390. https://doi.org/10.1016/i.jiheatmasstransfer.2018.05.043.
- Seyeux, A., Maurice, V., Klein, L.H., et al., 2008. Initiation of localized corrosion at the nanoscale by competitive dissolution and passivation of nickel surfaces. Electrochim. Acta 54 (2), 540–544. https://doi.org/10.1016/j.electacta.2008.07.033.
- Seyyedattar, M., Ghamartale, A., Zendehboudi, S., et al., 2023. Assessment of CO₂-Oil swelling behavior using molecular dynamics simulation: CO₂ utilization and storage implication. J. Mol. Liq. 379, 121582. https://doi.org/10.1016/j.molliq.2023.121582.
- Shalev-Shwartz, S., Zhang, T., 2013. Stochastic dual coordinate ascent methods for regularized loss minimization. J. Mach. Learn. Res. 14, 567–599. https://doi.org/ 10.48550/arXiv.1209.1873.
- Shang, Q.Y., Xia, S.Q., Cui, G.W., et al., 2017. Measurement and correlation of the interfacial tension for paraffin+CO₂ and (CO₂+N₂) mixture gas at elevated temperatures and pressures. Fluid Phase Equilib. 439, 18–23. https://doi.org/10.1016/j.fluid.2017.02.012.
- Shorten, C., Khoshgoftaar, T.M., 2019. A survey on image data augmentation for deep learning. J. Big Data 6 (1), 60. https://doi.org/10.1186/s40537-019-0197-0.
- Soleimani, M., Hill, R.J., van-de-Ven, T.G.M., 2013. Bubbles and drops on curved surfaces. Langmuir 29 (46), 14168–14177. https://doi.org/10.1021/la403088r.
- Span, R., Wagner, W., 1996. A new equation of state for carbon dioxide covering the fluid region from the triple-point temperature to 1100 K at pressures up to 800 MPa. J. Phys. Chem. Ref. Data 25, 1509–1596. https://doi.org/10.1063/1.555991.
- Su, H.X., Wang, H.T., Li, D.Y., et al., 2023. Diffusion and dissolution behaviors of CO₂, CH₄, and N₂ in heavy oil under high-temperature and -pressure conditions: insights into heavy oil production via multithermal fluid stimulation. Energy Fuels 37 (20), 15753–15767. https://doi.org/10.1021/acs.energyfuels.3c02749.
- Wang, P., Zhao, F.L., Huang, S.J., et al., 2021. Laboratory investigation on oil increment and water cut control of CO₂, N₂, and gas mixture huff-n-puff in edgewater fault-block reservoirs. J. Energy Resour. Technol. 143 (8), 083001. https://doi.org/10.1115/1.4048862.
- Wang, X.Q., Zhang, S.Y., Gu, Y.A., 2010. Four important onset pressures for mutual interactions between each of three crude oils and CO₂. J. Chem. Eng. Data 55 (10), 4390–4398. https://doi.org/10.1021/je1005664.
- Wang, Z.J., Zhu, J.Z., Li, S.Y., 2023. Novel strategy for reducing the minimum miscible pressure in a CO₂—oil system using nonionic surfactant: insights from molecular dynamics simulations. Appl. Energy 352, 121966. https://doi.org/10.1016/j.apenergy.2023.121966.
- Yang, D.Y., Gu, Y.A., 2005. Interfacial interactions between crude oil and CO₂ under reservoir conditions. Petrol. Sci. Technol. 23 (9–10), 1099–1112. https://doi.org/ 10.1081/lft-200035536.
- Yang, Y.F., Wan, J.Y., Shang, X.Y., et al., 2023. Molecular insights into fluid-solid interfacial tensions in water plus gas plus solid systems at various temperatures and pressures. J. Chem. Phys. 159 (9), 094701. https://doi.org/10.1063/ 5.0157657
- Yang, Z.H., Liu, X.L., Hua, Z., et al., 2015. Interfacial tension of CO₂ and crude oils under high pressure and temperature. Colloids Surfaces A-Physicochem. Eng. Aspects 482, 611–616. https://doi.org/10.1016/j.colsurfa.2015.05.058.
- Zhang, C., Li, Z.M., Sun, Q., et al., 2016. CO₂ foam properties and the stabilizing mechanism of sodium bis(2-ethylhexyl)-sulfosuccinate and hydrophobic nanoparticle mixtures. Soft Matter 12 (3), 946–956. https://doi.org/10.1039/
- Zhang, C., Xi, L.H., Wu, P.K., et al., 2020. A novel system for reducing CO₂-crude oil minimum miscibility pressure with CO₂-soluble surfactants. Fuel 281, 118690. https://doi.org/10.1016/j.fuel.2020.118690.
- Zhang, C., Gu, Z.H., Li, Z.Y., et al., 2024a. Influence of CO₂ on asphaltene adsorption dynamics at the oil—gas Interface: new insights into precipitation and aggregation processes. Fuel 375, 132592. https://doi.org/10.1016/j.fuel.2024.132592.
- Zhang, C., Li, P.F., Lun, Z.M., et al., 2024b. Unveiling the beneficial effects of N₂ as a CO₂ impurity on fluid-rock reactions during carbon sequestration in carbonate reservoir aquifers: challenging the notion of purer is always better. Environ. Sci. Technol. 58 (52), 22980–22991. https://doi.org/10.1021/acs.est.4c07453.
- Zhang, C., Liu, Y.L., Gu, Z.H., et al., 2024c. Chemicals-CO₂ mechanisms of inhibiting steam heat transfer and enhancing oil film strip: steam flow through the wall-adhering oil film surface in porous medium. Fuel 356, 129572. https://doi.org/10.1016/j.fuel.2023.129572.
- Zhang, K.Q., Tian, L., Liu, L.R., 2018. A new analysis of pressure dependence of the equilibrium interfacial tensions of different light crude oil-CO₂ systems. Int. J. Heat Mass Tran. 121, 503–513. https://doi.org/10.1016/j.ijheatmasstransfer.2018.01.014.
- Zhang, X., Li, L., Su, Y.L., et al., 2023. Microfluidic investigation on asphaltene interfaces attempts to carbon sequestration and leakage: oil-CO₂ phase interaction characteristics at ultrahigh temperature and pressure. Appl. Energy 348, 121518. https://doi.org/10.1016/j.apenergy.2023.121518.
- Zheng, H.M., Mahmoudzadeh, A., Amiri-Ramsheh, B., et al., 2023. Modeling viscosity of CO₂-N₂ gaseous mixtures using robust tree-based techniques: extra

- tree, random forest, GBoost and LightGBM. ACS Omega 8 (15), 13863-13875. https://doi.org/10.1021/acsomega.3c00228.
- Zolghadr, A., Escrochi, M., Ayatollahi, S., 2013a. Temperature and composition effect on CO₂ miscibility by interfacial tension measurement. J. Chem. Eng. Data 58
- (5), 1168–1175. https://doi.org/10.1021/je301283e.
 Zolghadr, A., Riazi, M., Escrochi, M., et al., 2013b. Investigating the effects of temperature, pressure, and paraffin groups on the N₂ miscibility in hydrocarbon liquids using the interfacial tension measurement method. Ind. Eng. Chem. Res.
- 52 (29), 9851–9857. https://doi.org/10.1021/ie401283q. Zuo, Y.X., Stenby, E.H., 1996. A linear gradient theory model for calculating interfacial tensions of mixtures. J. Colloid Interface Sci. 182 (1), 126–132. https:// doi.org/10.1006/jcis.1996.0443.
- Zuo, Y.X., Stenby, E.H., 1997. Calculation of interfacial tensions with gradient theory. Fluid Phase Equilib. 132 (1), 139–158. https://doi.org/10.1016/S0378-3812(96)